

BRASKI

DOE/ET-0058/6



Alloy Development for Irradiation Performance

Quarterly Progress Report
For Period Ending June 30, 1979

U.S. Department of Energy
Assistant Secretary for Energy Technology
Office of Fusion Energy

Printed in the United States of America. Available from
National Technical Information Service
U.S. Department of Commerce
5285 Port Royal Road, Springfield, Virginia 22161
NTIS price codes— Printed Copy: A06 Microfiche A01

This report was prepared as an account of work sponsored by an agency of the United States Government. Neither the United States Government nor any agency thereof, nor any of their employees, makes any warranty, express or implied, or assumes any legal liability or responsibility for the accuracy, completeness, or usefulness of any information, apparatus, product, or process disclosed, or represents that its use would not infringe privately owned rights. Reference herein to any specific commercial product, process, or service by tradename, trademark, manufacturer, or otherwise, does not necessarily constitute or imply its endorsement, recommendation, or favoring by the United States Government or any agency thereof. The views and opinions of authors expressed herein do not necessarily state or reflect those of the United States Government or any agency thereof.

DOE/ET-0058/6
Distribution
Category
UC-20, 20c

**ALLOY DEVELOPMENT FOR IRRADIATION PERFORMANCE QUARTERLY
PROGRESS REPORT FOR PERIOD ENDING JUNE 30, 1979**

Compiled and Edited by B. G. Ashdown, ORNL
from Contributions of Participating Laboratories

ARGONNE NATIONAL LABORATORY

GENERAL ATOMIC COMPANY

HANFORD ENGINEERING DEVELOPMENT LABORATORY

McDONNELL DOUGLAS ASTRONAUTICS COMPANY

NAVAL RESEARCH LABORATORY

OAK RIDGE NATIONAL LABORATORY

WESTINGHOUSE FUSION POWER SYSTEMS

Date Published: April 1980

Prepared by
OAK RIDGE NATIONAL LABORATORY
Oak Ridge, Tennessee 37830
operated by
UNION CARBIDE CORPORATION
for the
DEPARTMENT OF ENERGY
Under Contract No. W-7405-eng-26

FOREWORD

This report is the sixth in a series of Quarterly Technical Progress Reports on "*Alloy Development for Irradiation Performance*" (ADIP), which is one element of the Fusion Reactor Materials Program, conducted in support of the Magnetic Fusion Energy Program of the U.S. Department of Energy. Other elements of the Materials Program are:

- *Damage Analysis and Fundamental Studies (DAFS)*
- *Plasma-Materials Interaction (PMI)*
- *Special-Purpose Materials (SPM)*

The ADIP program element is a national effort composed of contributions from a number of National Laboratories and other government laboratories, universities, and industrial laboratories. It was organized by the Materials and Radiation Effects Branch, Office of Fusion Energy, DOE, and a Task Group on *Alloy Development for Irradiation Performance*, which operates under the auspices of that Branch. The purpose of this series of reports is to provide a working technical record of that effort for the use of the program participants, for the fusion energy program in general, and for the Department of Energy.

This report is organized along topical lines in parallel to a Program Plan of the same title so that activities and accomplishments may be followed readily relative to that Program Plan. Thus, the work of a given laboratory may appear throughout the report. Chapters 1, 2, 7, and 8 review activities on analysis and evaluation, test methods development, status of irradiation experiments, and corrosion testing and hydrogen permeation studies, respectively. These activities relate to each of the alloy development paths. Chapters 3, 4, 5, and 6 present the ongoing work on each alloy development path. The Table of Contents is annotated for the convenience of the reader.

This report has been compiled and edited under the guidance of the Chairman of the Task Group on *Alloy Development for Irradiation Performance*, E. E. Bloom, Oak Ridge National Laboratory, and his efforts, those of the supporting staff of ORNL and the many persons who made technical contributions are gratefully acknowledged. T. C. Reuther, Materials and Radiation Effects Branch, is the Department of Energy Counterpart to the Task Group Chairman and has responsibility for the ADIP Program within DOE.

Klaus M. Zwilsky, Chief,
Materials and Radiation Effects Branch
Office of Fusion Energy

CONTENTS

FOREWORD.		iii
1. ANALYSIS AND EVALUATION STUDIES		1
1.1 Establishment of a Materials Handbook for Fusion Reactor Systems (McDonnell Douglas)		2
<p style="margin-left: 40px;"><i>The Materials and Radiation Effects branch of the Office of Fusion Energy is in the process of developing a Materials Handbook for Fusion Reactor Systems (MHFS). The handbook will be similar in format to the Nuclear Systems Materials Handbook developed for the breeder reactor program but will contain materials and material properties that are relevant to the fusion program. The contents of the MHFS will initially be limited to the first wall and blanket structural materials, and will be made available to those involved in fusion design and system studies. Based on information received from key personnel currently working on the ETF, INTOR, and the commercial tokamak projects, the structural materials of most interest to them are 20% cold worked 316 stainless steel, ferritic alloys, and titanium alloys. Therefore, for the near term (next 6 months) efforts will be directed to develop data sheets on these alloys for inclusion in the handbook.</i></p>		
1.2 Ferritic Stainless Steels for Fusion Applications (General Atomic Company)		a
<p style="margin-left: 40px;"><i>The applications base and performance history of 9-12 Cr steels pertinent to use in fusion reactors was assessed. The most significant long-term high temperature usage has been in European fossil-fired power plants, where performance of welded structures has been excellent. A detailed metallurgical evaluation by General Atomic Co./Sulzer Brothers of an HT-9 superheater tube after 80,000 hours of service indicated good thermal stability, excellent residual mechanical properties, and reduced but significant impact toughness.</i></p> <p style="margin-left: 40px;"><i>The key issues for the application of these steels in fusion systems were identified as the adequacy of fracture resistance, performance in the fusion irradiation environment, and the acceptability of fabrication/welding characteristics. The results of a data base assessment of candidate alloys, commercial UT-9 (12 Cr-1 Mo) and developmental 9 Cr-1 Mo, indicated significant need for irradiation performance data.</i></p>		
2. TEST MATRICES AND TEST METHODS DEVELOPMENT		17
2.1 Elevated Temperature Fatigue Crack Growth Testing Using Miniature Specimen Technology (Hanford Engineering Development Laboratory)		18

Elevated temperature fatigue crack growth data has been generated using an electrical potential technique of monitoring crack extension in miniature center-cracked-tension specimens. The technique produced reliable accurate results at 316 and 260°C when compared with data generated from conventional compact tension specimens.

2.2 Status of an In-Reactor Fatigue Crack Propagation Experiment (Hanford Engineering Development Laboratory) . . . 28

The design of an in-reactor fatigue machine capable of performing tension/tension cycling on a chain of center-cracked-tension specimens in the ORR is nearing completion. A tentative test matrix has been established using the Path A Reference Alloy, 20% cold work 316 stainless steel.

2.3 Neutronic Design of Spectral Tailoring Experiments (ORNL) . . . , 35

We have calculated the effect of a tantalum core piece in the ORR on the thermal neutron flux and displacement rate in an enclosed experimental capsule. The large thermal capture cross section of tantalum [about $2.0 \times 10^{-27} \text{ m}^2$ (20 b)] reduces not only the thermal flux but also the displacement rate in the experimental capsule as a result of localized reduction in the number of fissions. This reduction in displacement rate can be partly offset by increasing the fuel loading in adjacent core pieces.

2.4 Design of Irradiation Experiments in ORR Using Spectral Tailoring and Reencapsulation (ORNL) 38

We have designed and drawn the two experiments ORR-MFE-4A and ORR-MFE-4B. The first experiment will contain specimens at 300 and 400°C, and the second will contain specimens at 500 and 600°C. Parts are being fabricated for a bench test of the experiment, and a gamma heat measuring experiment is awaiting irradiation.

3. PATH A ALLOY DEVELOPMENT —AUSTENITIC STAINLESS STEELS 41

3.1 Low-Cycle Fatigue Behavior of 20%-Cold-Worked Type 316 Stainless Steel After Irradiation in the HFIR (ORNL) . . . 42

Specimens of 20%-cold-worked type 316 stainless steel were irradiated in the High Flux Isotope Reactor (HFIR) to fluences of 0.85 to $1.9 \times 10^{26} \text{ n/m}^2$, resulting in displacement levels of 7 to 15 dpa and helium contents of 250 to 860 at. ppm. Fully reversed strain controlled fatigue tests were performed with strain ranges of 0.40 to 2.0%. The specimens were irradiated and tested at 430°C and tested in a vacuum at a pressure below 10^{-4} Pa . The fatigue life was reduced by factors of 3 to 10. We are studying fracture surfaces and will subsequently report the results.

3.2 Microstructural Design for Fusion First-Wall Applications and Recommendations for Thermal-Mechanical Preirradiation Treatments (ORNL) 48

Previous work [including High Flux Isotope Reactor (HFIR) tests] on the effects of helium in metals indicates that the chances of maintaining good mechanical response in a fusion reactor depend on keeping helium away from the grain boundaries and trapping it intragranularly. Swelling from helium bubble formation is inevitable, but the finest helium distribution will minimize swelling. We propose a matrix of desirable preirradiation microstructures for the PCA based upon responses of type 316 stainless steel or type 316 modified with titanium to HFIR irradiation. Desirable microstructures result from a combination of grain boundary precipitation, cold work, and distribution of titanium-rich MC. We also discuss thermal-mechanical treatments to produce these microstructures. Further work includes completing the fabrication procedures on which microstructural homogeneity and control intimately depend.

4. PATH B ALLOY DEVELOPMENT — HIGHER STRENGTH Fe-Ni-Cr ALLOYS . . . 57

5. PATH C ALLOY DEVELOPMENT — REACTIVE AND REFRACTORY ALLOYS . . . 59

5.1 Preparation of Vanadium and Niobium Path C Scoping Alloys (Westinghouse Electric Corporation and ORNL) 61

Three vanadium alloy and two niobium alloy compositions are being prepared for consumable arc melting and processing to plate, sheet, and rod for the Fusion Materials Stockpile. These are the Path C (V, Nb) Scoping Alloys selected for initial evaluations as candidate fusion reactor structural materials. All melting and primary metal working operations have been completed. Extrusions to sheet bar and round bar were accomplished without difficulty; final rolling and swaging are underway. Delivery of various product forms will begin by approximately mid-August with final delivery of all materials to the Fusion Materials Stockpile at Oak Ridge expected to be complete by mid-October.

6. PATH D ALLOY DEVELOPMENT — INNOVATIVE MATERIAL CONCEPTS 65

7. STATUS OF IRRADIATION EXPERIMENTS AND MATERIALS INVENTORY . . . 67

7.1 Irradiation Experiment Status and Schedule (ORNL) 68

The schedule for irradiation experiments being conducted by the Alloy Development Program is presented.

7.2 ETM Research Materials Inventory (ORNL and McDonnell Douglas) 75

Procurement status and inventory of Path A, B, and C Alloys are reported.

8. CORROSION TESTING AND HYDROGEN PERMEATION STUDIES 81

8.1 Corrosion in Static Lithium: Further Tests on Corrosion Inhibition of Type 316 Stainless Steel and the Corrosion of Weld Specimens of Type 316 Stainless Steel and Path B-Like Materials (ORNL) 82

Type 316 stainless steel was exposed to Li-2 wt % N-5 wt % Al between 500 and 700°C for 1000 h. While this amount of nitrogen normally enhances attack of type 316 stainless steel, the addition of aluminum prevented significant corrosion. We studied the corrosion resistance of unstressed welds of type 316 stainless steel and two Path B-like alloys (alloys 800 and 600) in lithium. In general, after 1000 h at 500 and 600°C the welds of the three were as compatible with static as-purified lithium as their respective base alloys.

8.2 Mass Transfer Deposits in Lithium-Type 316 Stainless Steel Thermal-Convection Loops (ORNL) 89

We studied the morphology and composition of mass transfer deposits in lithium-type 316 stainless steel thermal-convection loops (TCLs). Initially the deposits were needle-like crystals of nearly pure chromium. After longer operating times the deposits were blocky, and their composition varied as a function of their distance above the original surface. The later-formed deposits contained iron, chromium, and nickel. However, they were enriched in chromium and nickel relative to the concentrations of these two elements in the stainless steel. A plug that formed in a TCL after 9000 h consisted of lithium and a tangle of chromium crystals.

8.3 Hydrogen Dissolution and Permeation Characteristics of Titanium-Base Alloys (Argonne National Laboratory) 95

The hydrogen permeation characteristics of an anodized sample of Ti-6Al-4V were measured from 450 to 665°C for hydrogen driving pressures in the range from 0.2 to 1.7 Pa. The permeability of the anodized sample was found to be about the same as that of the ion-nitride coated sample of Ti-6Al-4V studied previously, and about an order of magnitude lower than that of pure Ti-6Al-4V. A least-squares analysis was conducted on data for pure Ti-6Al-4V, ion-nitride-coated Ti-6Al-4V, and anodized Ti-6Al-4V wherein the preexponential term and the activation energy were varied independently for each sample but a common refined value for the pressure exponent was sought. It is clear from the results of this analysis that the coating procedures caused a measurable but far less than desirable reduction in the permeability of Ti-6Al-4V. The optimized pressure exponent, 0.64, suggests that the normally-assumed bulk-diffusion-limited permeation mechanism is being affected or perhaps totally superseded by another mechanism involving the surfaces of the alloy.

8.4	Vanadium Alloy/Lithium Pumped Loop Studies (Argonne National Laboratory)	99
-----	------------------------------------------------------------------------------------	----

The stainless-steel-clad *vanadium-15% chromium* alloy loop for studies of circulating liquid lithium has continued to operate through the third quarter of FY-1979. This 0.5-liter-capacity, forced circulation loop is being used in investigations of (1) the distribution of non-metallic elements in *lithium/refractory metal* systems and (2) effects of a lithium environment on the mechanical properties of selected refractory metals. Exposure of *zirconium* foil to lithium at both 673 and 873 K resulted in significant pickup of nitrogen by the zirconium and a corresponding reduction of the nitrogen concentration in *lithium*.

1. ANALYSIS AND EVALUATION STUDIES

The designs for power-producing fusion reactors are in a very embryonic and rapidly changing state. Requirements for materials performance are thus not well defined. However, regardless of the final designs, the environment will clearly be extremely demanding on materials in regions of high neutron flux. **One** cannot identify a class of alloys on which the development efforts should focus — thus the parallel paths of the Alloy Development Program. The combination of reactor designs that are evolving and the necessity for including alloys with widely different physical, chemical, and mechanical properties in the program could lead to an impossibly large number of potential problems and possible solutions. Analysis and evaluation studies are an essential part of the Alloy Development Program in order to translate fusion reactor performance goals into material property requirements and to identify crucial and generic problems on which development activities should be focused. As the Alloy Development Program proceeds and a better understanding of the behavior of materials in potential fusion reactor environments is attained, these studies will also identify problems that will necessitate design solutions.

1.1 ESTABLISHMENT OF A MATERIALS HANDBOOK FOR FUSION REACTOR SYSTEMS - J. W. Davis (McDonnell Douglas)

1.1.1 ADIP Task

Task Number 1.A.1 - Define Material Property Requirements and Make Structural Life Predictions. ,

1.1.2 Objective

To establish a materials data book for use in the design and analysis of near term and conceptual fusion reactor systems.

1.1.3 Summary

The Materials and Radiation Effects branch of the Office of Fusion Energy is in the process of developing a Materials Handbook for Fusion Reactor Systems (MHFS). The handbook will be similar in format to the Nuclear Systems Materials Handbook developed for the breeder reactor program but will contain materials and material properties that are relevant to the fusion program. The contents of the MHFS will initially be limited to the first wall and blanket structural materials, and will be made available to those involved in fusion design and system studies. Based on information received from key personnel currently working on the ETF, INTOR, and the commercial tokamak projects, the structural materials of most interest to them are 20% cold worked 316 stainless steel, ferritic alloys, and titanium alloys. Therefore, for the near term (next 6 months) efforts will be directed to develop data sheets on these alloys for inclusion in the handbook.

1.1.4 Progress and Status

The design and analysis of various components in near term and commercial fusion reactor concepts has reached the level of sophistication that a consistent source of materials data is needed, particularly with respect to radiation damage. Recognizing this need, the Materials and Radiation Effects Branch of the Office of Fusion Energy is establishing a Materials Handbook for Fusion Reactor Systems (MHFS). This handbook will be similar in format to the Nuclear Systems Materials Handbook (NSMH)

but will cover materials and data that may not be of interest to the general breeder reactor community. Publication and distribution of this data book will be handled through R. A. Moen of the Materials Applications branch of the Hanford Engineering Development laboratory while preparation of the data sheets will be handled by a subtask group of ADIP. The relationship of this subtask group to ADIP and in turn to the NSMH committee is shown in Figure 1.1.1. As part of the Analysis and Evaluation Subtask group the committee for the MHFS will be responsive to not only the fusion design needs but also the improvements in materials properties or new data that is being developed through the ADIP program.

The success and acceptance of the MHFS by the various fusion projects is dependent not only on the quality of the data but also upon the depth and understanding of material behavior that went into the preparation of the data sheets. Therefore, this handbook cannot be the product of any one individual or any one organization but must reflect the contributions of a number of organizations. Towards this end a committee for the MHFS was established with participants from 7 different laboratory and industrial organizations.

Each of the members of this committee will be responsible for the preparation of part of the handbook. Figure 1.1.2 shows the tentative members of this committee along with their area of responsibility and the organization they are from.

The analysis and Evaluation Subtask group will receive inputs through both the ADIP organization and recommendations or suggestions for data needs from the design projects such as ETF and Commercial Tokamak. Based on these inputs the Analysis and Evaluation Subtask group will establish data needs and priorities, with ADIP Task Group Approval. With the establishment of data priorities, the key individuals of the data book committee will be asked to prepare the necessary data sheets. That individual has the option of preparing the data sheets and supporting documentation on his own or to convene a small working group to assist in the preparation of the data sheets. The prepared data sheets will be submitted to the Chairman of the MHFS Committee who will coordinate the review and approval process. The review will be accomplished through a review group consisting of appropriate members of the MHFS Committee and

FIGURE 1.1.1 MATERIALS HANDBOOK FOR FUSION REACTOR SYSTEMS FUNCTIONAL ORGANIZATION

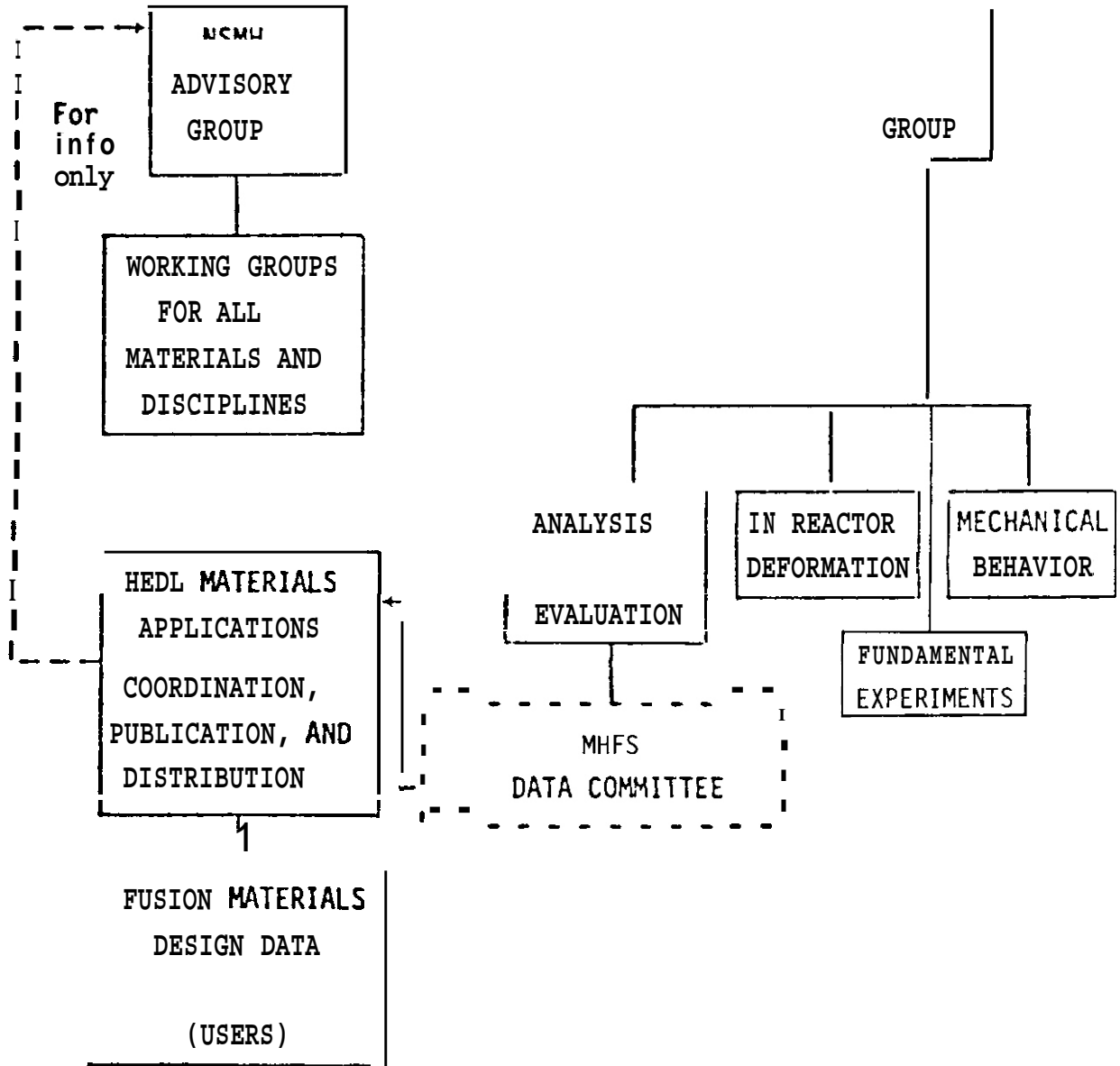


FIGURE 1.1.2 MATERIALS HANDBOOK FOR FUSION REACTOR
SYSTEM DATA COMMITTEE MEMBERS

Chairman - J. W. Davis

<u>Members</u>	<u>Organization</u>	<u>Area of Responsibility</u>
F. W. Wiffen	ORNL	PATH A, irradiated
D. L. Smith	ANL	PATH A, unirradiated
J. J. Holmes	HEDL	PATH B , irradiated
S. M. Rosenwasser	GA	PATH B, unirradiated
R. E. Gold	Westinghouse	PATH C, irradiated
J. W. Davis/R. E. Gold	MDAC/Westinghouse	PATH C, unirradiated
J. J. Holmes	HEDL	PATH D (ferritic) irradiated
S. M. Rosenwasser	GA	PATH D (ferritic) unirradiated
J. H. DeVan	DRNL	Compatibility - Coolant
D. L. Smith	ANL	Compatibility - Breeder Material
V. A. Maroni	ANL	Tritium Transport & Retention
D. J. Michel	NRL	Fracture Mechanics Properties

people outside the committee who may be designers or structural analysts in order to achieve a balanced review. This review group will also have a Chairman who will be a member of the MHFS Committee and will be responsible for coordinating the results of the reviewers and make recommendations on the disposition of the data sheet. The Chairman of the MHFS will then review these comments and take the necessary action, either to return the data sheet to the preparer or forward it to HEDL for printing and distribution to the handbook holders.

Initially data in the MHFS will be limited to the first wall and blanket structural materials and as the data book develops expanded to include coolants and breeding materials. The near term objectives, i.e., 6-8 months, is to have the handbook contain unirradiated data sheets on 20% cold worked 316 stainless steel, ferritic alloys (HT-9, and 9 Cr-1Mo), and titanium alloys Ti-6Al-4V and Ti-6242s and irradiated data sheets on 20% cold worked 316 stainless steel. The irradiated data sheets will essentially be based on existing data but modified to account for transmuted helium. If possible, the existing predictive equations for swelling and irradiation creep of 316 will be modified for fusion use.

During this quarter the effort has been directed towards establishing the MHFS Committee, determining the title of the book and its color, establishing a distribution list for potential handbook users and to determine a priority for inclusion of materials in the handbook.

1.1.5 Conclusions and Future Work

Based on discussions with OFE and various members of ADIP, the title of the handbook was selected to be Materials Handbook for Fusion Reactor Systems and will bear the documentation number DOE/TIC-10122. It will be dark blue in color and should be available sometime in October.

A tentative list of recipients of the handbook has been prepared and letters announcing the formation of the book has been distributed. Those wishing to receive copies of the book and have not received letters indicating that they are on the distribution list should contact R. A. Moen at HEDL. The tentative distribution is over 70 individuals representing 33 organizations involved in fusion related studies.

Discussions with key personnel involved in the ETF, INTOR, and Commercial Tokamak studies have revealed that the alloys they are currently interested in are **316** stainless steel, ferritic steels, and titanium alloys. Therefore for the near term (next 6 months) effort will be directed toward preparing data sheets on these alloys **in** order of priority as they are listed above.

1.2 FERRITIC STAINLESS STEELS FOR FUSION APPLICATIONS - L. D. Thompson and S. N. Rosenwasser

1.2.1 ADIP Task

ADIP Task I.A.1, Define material property requirements and make structural life predictions.

1.2.2 Objective

The objective of this study is to assess the feasibility of incorporating ferromagnetic (martensitic) steels in fusion reactor designs and to evaluate the advantages of this class of material with respect to first wall/blanket lifetime. The pertinent experience base is being evaluated, and the irradiated and unirradiated property data needed for the application of ferritic stainless steels in fusion designs are being defined as part of this task.

1.2.3 Summary

The applications base and performance history of 9-12 Cr steels pertinent to **use** in fusion reactors was assessed. The most significant long-term high temperature usage has been in European fossil-fired power plants, where performance of welded structures has been excellent. A detailed metallurgical evaluation by General Atomic Co./Sulzer Brothers of an HT-9 superheater tube after 80,000 hours of service indicated good thermal stability, excellent residual mechanical properties, and reduced but significant impact toughness.

The key issues for the application of these steels in fusion systems were identified as the adequacy of fracture resistance; performance in the fusion irradiation **environment**, and the acceptability of fabrication/welding characteristics. The results of a data base assessment of candidate alloys, commercial HT-9 (12 Cr-1 Mo) and developmental 9 Cr-1 Mo, indicated significant need for irradiation performance data.

1.2.4 Progress and Status

The work during this reporting period emphasized an assessment of

the application experience and performance of 9-12 Cr steels, a detailed metallurgical evaluation of an HT-9 superheater tube after 80,000 hours service in a German power plant, and an identification of major issues/data needs for use of martensitic steels in fusion component designs. The results of this work are discussed below.

1.2.4.1 Application Experience

The class of 9-12 Cr steels has been used extensively in power generation applications throughout Europe for over 25 years. While most of these applications have been directed towards superheaters, reheaters, and evaporators for oil- and coal-fired power plants, much experience and performance history information pertinent *to* fusion application has been generated. In addition to fossil power plant applications, this class of steels has been employed in nuclear power plants. In the Hinkley Point "B" AGR reactor in the United Kingdom, superheaters and reheaters are 9 and 12 Cr steels.' In the U.S., the Fort St. Vrain HTGR employs standard 410 and 422 (12 Cr) stainless steel grades in the helium circulators and compressors.' Other applications have included gas and steam turbine components, aircraft and missile thin-wall pressure vessels, and petroleum industry pressure vessel linings.³

Other proposed nuclear applications for 9-12 Cr steels, presently under consideration, include ducts, cladding, and steam generators for the U.S. LMFR and GCFR, steam generators for the Japanese FBR, ducts and steam generators for the French Super Phenix, steam generators, helium-helium heat exchangers, helium circulators, and steam piping for the U.S. HTGR, and steam generators for the U.S. LWR.

Two of the largest users for fossil plants in Europe have been Sulzer Brothers (Switzerland) and the United Kingdom Central Electricity Generating Board (CEGB). Table 1.2.1 indicates the performance and failure histories for these two organizations. In the U.K., CEGB has 25 operating fossil power plants which use 9 and 12 Cr steels.¹ Application temperatures were as high as 850°C, but successful long-term operation temperatures were limited *to* the range of 600°-650°C maximum. At the

Table 1.2.1. Foreign Usage and Performance of
9-12 Cr Steels in Fossil Power Plants

LOCATION	USAGE	ALLOY	TEMPERATURE (°C)	SERVICE STATUS (K.Hrs)	FAILURE HISTORY
UK	13 PLANTS	9 CrMo (V)	450 - 660	110	1 FAULTY WELD 1 FAULTY WELD REPAIR FIRESIDE CORROSION
	12 PLANTS	12 CrMo	430 - 850	45	OVERHEATING > 650°C
AUSTRIA BELGIUM CZECHOSLOVAKIA GERMANY SWITZERLAND TURKEY YUGOSLAVIA	96 TONS	9 CrMo	610	110	1 FAULTY WELD REPAIR
	> 250 TONS	12 CrMo (V, W)	610	130	FIRESIDE CORROSION

higher temperatures, overheating contributed to a significant amount of creep damage with correspondingly shorter rupture lives. Of particular interest is the relatively few weld failures. Welding must be performed following a careful procedure involving pre- and post-weld heat treatments. Only two failures have been reported which related directly to welding.

In the lower part of Table 1.2.1 the countries and total tonnages are reported for Sulzer Brothers fossil power plants.⁴ Again, excellent operating performance with only limited failures has been observed.

1.2.4.2 Metallurgical Performance Evaluation of HT-9

In order to quantify the long-term high-temperature service performance of candidate martensitic stainless steel for fusion application, General Atomic, in conjunction with Sulzer, evaluated the behavior of HT-9 (DINX20CrMoVW121) superheater tubing from a welded boiler in the Reutlingen, Germany coal-fired power plant. Tubes were removed from service after 80,000 hours at temperatures near 600°C. In addition to 720 normal operating starts/shutdowns (50 from room temperature), the tube had also experienced six off nominal thermal shocks related to

power failures at the plant. The tubes were subjected to relatively low stresses of approximately 20–50 MPa.

The interrupted service evaluation included stress–rupture, tensile in the temperature range of 23°–600°C, Charpy V–notch impact toughness, and microstructural evaluation. The properties of unexposed tubing were determined simultaneously for comparison.

Figure 1.2.1 shows the curves obtained in the stress–rupture tests with stress plotted as a function of the Larson–Miller parameters?

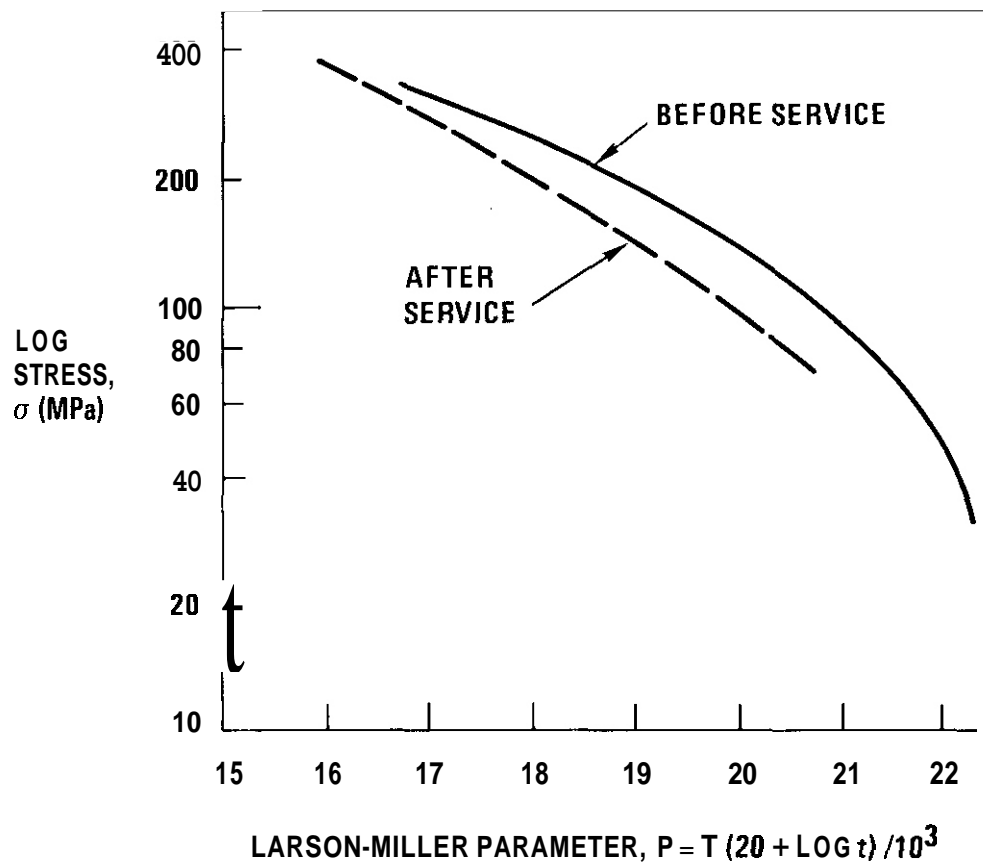
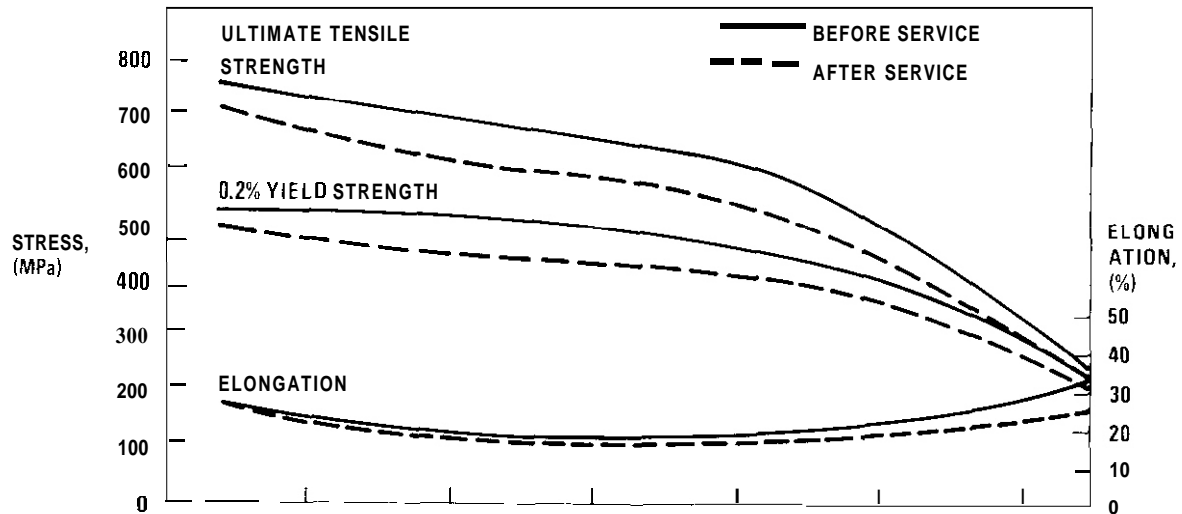


Fig. 1.2.1. Effect of 80,000 hour, 600°C Service Exposure on HT-9 Stress–Rupture Properties

Overaging of carbides after 80,000 hours of in–service exposure decreased stress–rupture lifetimes, particularly at the higher stress levels. As indicated by Fig. 1.2.1, the residual creep properties were quite good

compared to properties before service. It should also be mentioned that total creep strains did not change significantly. Figure 2 shows the



room- and elevated-temperature tensile properties determined and, again, strength properties were only slightly reduced after long-term service and the tensile ductilities remained quite close to pre-service values over the entire test temperature range. Figure 1.2.3 shows the impact toughness values obtained at 22° and -45°C, for half-width specimens. Impact toughness decreased, however, substantial toughness remained even at -45°C. This alloy (HT-9) undergoes a transition in impact fracture behavior from ductile to brittle with decreasing temperature, and following the service exposure, the ductile-to-brittle transition temperature (DBTT) shifted to a somewhat higher temperature, although the precise DBTT was not determined in these tests.

Transmission electron microscopy was employed to study the microstructural changes occurring with the service exposure. Overall structural stability appeared to be excellent with the most prominent feature noted as the enhanced precipitation of $M_{23}C_6$ carbides at

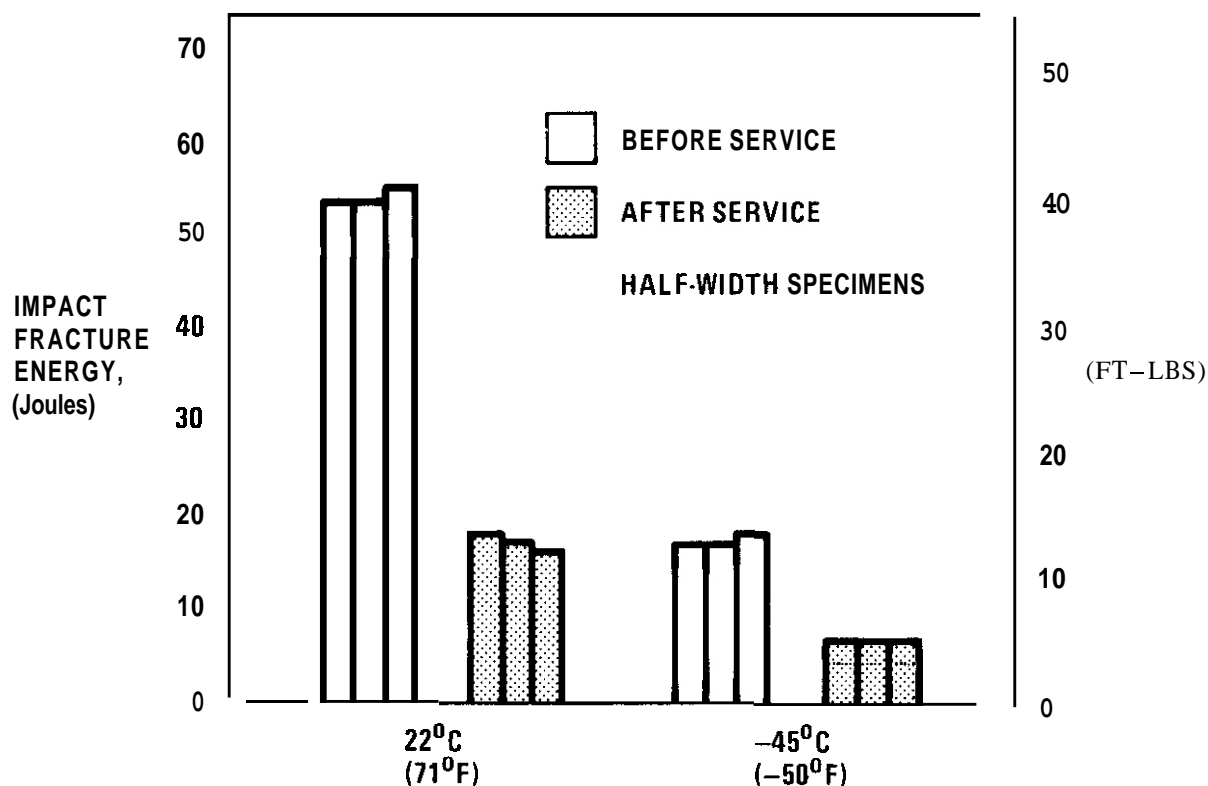


Fig. 1.2.3. Effect of 80,000 hour, 600°C Service Exposure on HT-9 Impact Properties

martensite interlath boundaries. Some precipitation of a Fe_2Mo laves phase was also noted but was not found to be morphologically detrimental to the mechanical properties. The decrease in impact toughness properties was most likely associated with the carbide precipitation. Thus, the effects of a long-term service exposure did *not* lead to dramatic reductions in mechanical properties, consistent with the overall good thermal stability of HT-9.

1.2.4.3 Key Issues and Major Data Requirements

The key issues in evaluating the potential of the martensitic stainless steels for fusion applications were identified as the fracture resistance (the change in fracture toughness with decreasing temperature), the effect of simulated fusion irradiation on the mechanical properties, and the weldability and fabricability pertinent to the construction and

maintenance of fusion reactor components. If these issues are resolved it is possible that martensitic stainless steels could be selected for the construction of some components in the Engineering Test Facility (ETF).

An assessment of the data base which exists for HT-9 and the developmental Combustion Engineering/ORNL 9 Cr-1 Mo alloy was completed. Table 1.2.2 shows the properties of interest and the status of reported properties. It is obvious that a comprehensive testing program, with emphasis on fracture related properties, irradiation performance, and fabrication feasibility issues will be required to fully assess the potential of martensitic steels for ETE' and subsequent fusion devices.

Table 1.2.2. Current Data Base for HT-9 and Modified 9 Cr-1 Mo

PROPERTY	HT-		MODIFIED	
	IRRADIATED	RADIATED	IRRADIATED	RADIATED
TENSILE	○	⊗	●	○
STRESS-RUPTURE	○	○	⊗	○
CREEP	⊗	●	●	○
VOID SWELLING		⊗		○
CREEP-FATIGUE	○	○	⊗	○
FATIGUE CRACK GROWTH	○	○	○	○
FRACTURE TOUGHNESS	○	○	○	○
IMPACT TOUGHNESS	●	⊗	⊗	○
WELD PROPERTIES	⊗	○	●	○
COOLANT COMPATIBILITY	●	○	○	○
PHYSICAL PROPERTIES	○	○	●	○
MAGNETIC PROPERTIES	⊗	○	⊗	○

○ NONE REPORTED ⊗ INSUFFICIENT FOR ETF DESIGN ● SUFFICIENT FOR ETF DESIGN

1.2.5 References

1. Wyatt, L. M., "The Performance of Cr-Mo Steels in the Boilers of CEGB Power Stations," in Ferritic Steels for Fast Reactor Steam Generators, edited by S. F. Pugh and E. A. Little, 1978, proceedings of an International Conference held by the British Nuclear Energy Society at the Institution of Civil Engineers, London, May 30 through June 2, 1977.
2. Smith, A., General Atomic Company, private communication.
3. Briggs, J. Z., and Parker, T. D., The Super 12% Cr Steels, Climax Molybdenum Company, Ann Arbor, Michigan, 1965.
4. Fricker, H., "Sulzer Experience with High Chromium Ferritic Steels," Report TA 2730, Sulzer Brothers, Switzerland, February, 1977.
5. Walser, B., "The Metallurgical and Mechanical Properties of X20CrMoWV121 After Service Exposure in a Fossil Fired Boiler," Report 222/1511, Sulzer Brothers, Switzerland, January, 1977.

2. TEST MATRICES AND TEST METHODS DEVELOPMENT

An important part of the alloy development effort is the definition of test matrices and development of test methods. The alloy development strategy will proceed through stages requiring tests of generally increasing difficulty and complexity.

1. Scoping tests will be used to make relative judgments between materials and metallurgical conditions and to identify critical properties. Such tests, which will be used where large numbers of variables are involved, must be rapid, simple, and decisive.

2. Developmental tests will be used for optimization of the Prime Candidate Alloys. They will be broader and more extensive than the scoping tests. In-reactor testing will be an important part of this work.

3. Engineering property tests will be devised to provide the broad data base needed for reactor design.

2.1 ELEVATED TEMPERATURE FATIGUE CRACK GROWTH TESTING USING MINIATURE SPECIMEN TECHNOLOGY - D. A. Mervyn (Hanford Engineering Development Laboratory).

2.1.1 ADIP Task

Task I.A.2, define *test* matrices and test procedures.

2.1.2 Objective

An electrical potential technique of measuring crack growth has been adapted to high temperature fatigue testing on miniature center-cracked-tension specimens in an effort to develop the technology required *to* characterize the post-irradiation fatigue crack growth behavior of fusion firstwall materials.

2.1.3 Summary

Elevated temperature fatigue crack growth data has been generated using an electrical potential technique of monitoring crack extension in miniature center-cracked-tension specimens. The technique produced reliable accurate results at 316 and 260°C when compared with data generated from conventional compact tension specimens.

2.1.4 Progress and Status

2.1.4.1 Introduction

Current magnetic fusion reactor design concepts require that the fatigue behavior of candidate first wall materials be characterized. Fatigue crack growth may, in fact, be the design limiting factor in these cyclic reactor concepts given the inevitable presence of crack-like flaws in fabricated sheet structures. Miniature specimen technology has been developed to provide the large data base necessary *to* characterize irradiation effects on the fatigue crack growth behavior.

This technology is based on a miniature weldable center-cracked-tension (CCT) specimen and an electrical potential technique of measuring crack length. The technique, test set up description and ambient temperature calibration data were reported previously.² Miniature specimen

fatigue crack growth data, obtained visually, has been compared to conventional data,³ Figure 2.1.1. The miniature specimen, Type 3, produced the same results as ten conventional specimen geometries. This report describes further testing which was conducted to confirm the validity of using the electrical potential technique at elevated temperatures.

2.1.4.2 Experimental Technique

Testing was performed in air at 260°C and 316°C and was compared to results obtained from a conventional compact tension (CT) specimen.¹ Type 316 SS specimens were employed for both the 260 and 316°C tests. To eliminate the effect of thermal emf's on the measured potentials, 0.13mm (0.005 inch), 316 SS wire probes were spot welded to the specimens. These probes were joined to larger 0.76mm (0.030 inch) 316 SS wire leading out of the furnace to a junction box, Figure 2.1.2. The specimens were cycled using a MTS feedback - controlled test machine using load as the control parameter. The 260°C specimen was cycled at 300 lbs. maximum load and the 316°C specimen at 350 lbs, maximum load. Both tests were conducted at a load ratio (R) of 0.05 and frequency of 15 Hz. A resistance heating clamshell furnace was employed for the tests.

2.1.4.3 Results

Crack length measurements were made at temperature using the electrical potential method at a constant current of 5 and 10 amps. These measurements were confirmed by daily visual measurements at room temperature using a traveling microscope.

The experimental technique utilized in this investigation consists of measuring two potential drops across the crack, Figure 2.1.2. Potential probes are placed so that one voltage, V_2 , is extremely sensitive to small crack extension. Another voltage, V_1 , is measured to account for changes in current and resistivity. By calculating a ratio of these voltages, V_1/V_2 , potential drops due to time dependent phase and structural changes as well as long term current fluctuations are eliminated. Simultaneous measurement of two potential drops eliminates time consuming theoretical and individual specimen calibrations required in previous experiments.^{4,5,6}

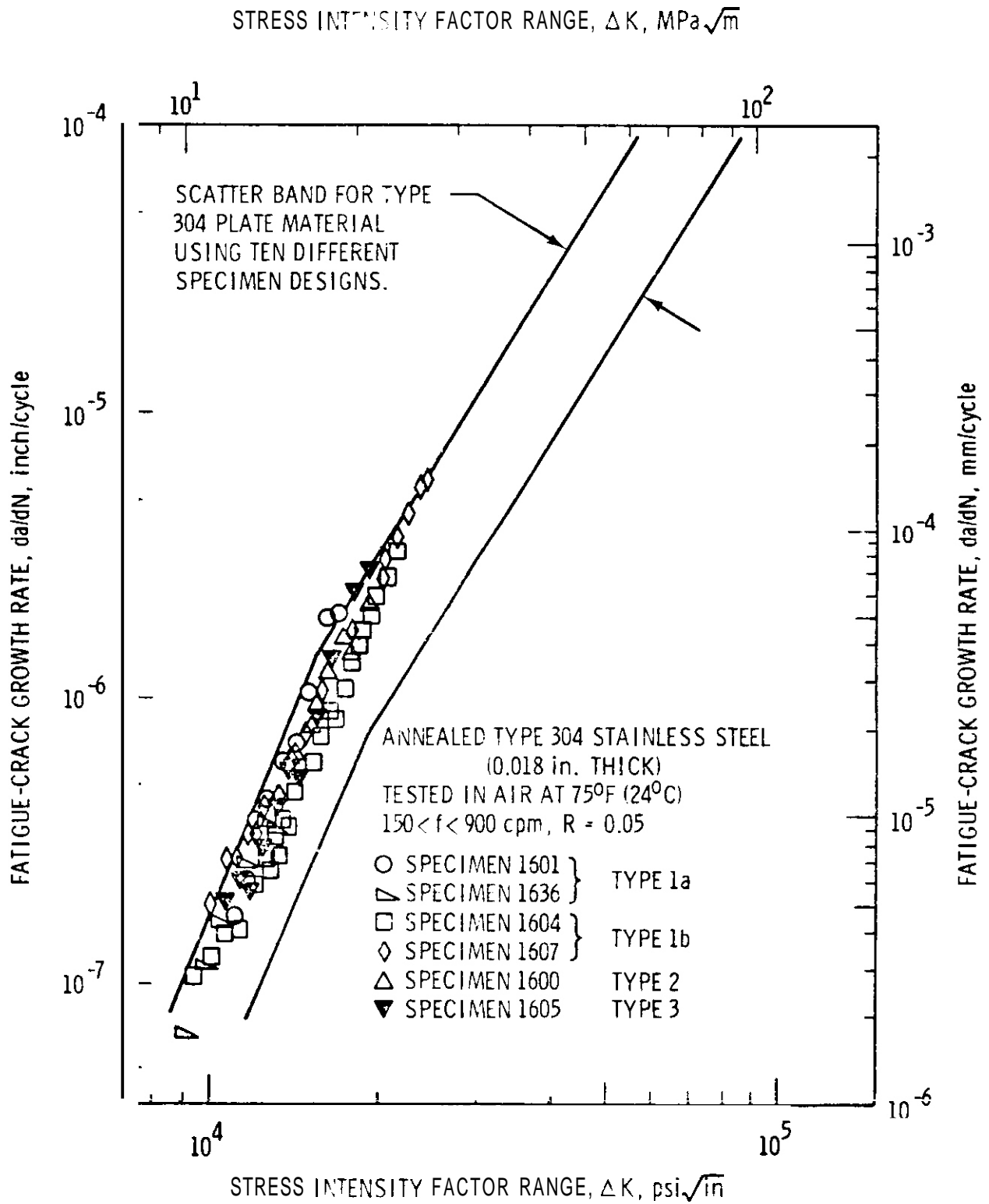


Figure 2.1.1. Fatigue Crack Growth Rate for Various Specimen Geometries

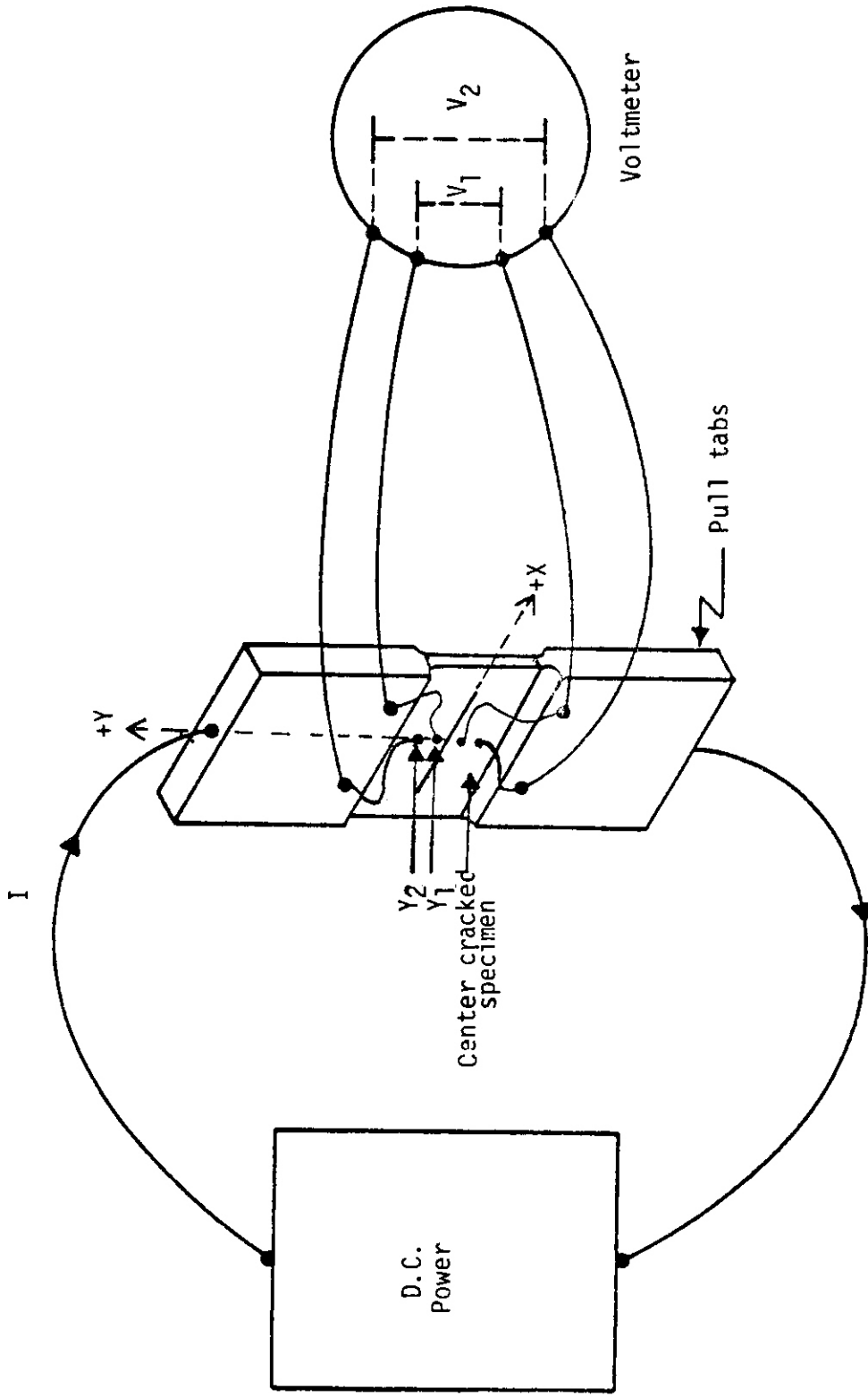


Figure 2.1.2 Crack Measurement Details

Still, questions do arise when using electrical potential measurements at elevated temperatures. Other investigators have found that thermal emf's which fluctuate with slight temperature changes can interfere with crack growth measurements.⁷ In this investigation, the effect of thermal emf's was reduced by using probes of similar composition as the specimen. The sensitivity of the electrical potential measurements in a relationship to the thermal emf's was examined by measuring V_1/V_2 at 5 and 10 amps at 260°C and 25°C, and by taking open circuit voltage measurements of the system to monitor fluctuations in thermal emf's. This was done to determine whether the accuracy of the potential measurements was a function of the applied current and whether increasing the input current would allow measurements to be made in materials where thermal emf's could not be eliminated. It was postulated that by increasing the current and, hence, the magnitude of the potential drop, thermal emf's would become a smaller proportion of the potential measurements.

Figure 2.1.3 shows the effect of current on the potential drop measurements. For 316 SS, current values in the range of 5 to 10 amps had no effect on the sensitivity of the measurements. Thermal emf's were found to be less than .3% of the measured potentials at both 5 and 10 amps. Resistance heating of the specimen was observed at input currents greater than 10 amps.

The ultimate test of testing technique is the generation of consistent data, Figure 2.1.4 shows the results of the test at 260°C on 316 CW SS. Both optical and electrical potential crack growth rate measurements are shown. Over the da/dN versus AK region investigated, both measurements gave the same results. An additional test was performed at 316°C to allow data generated using the potential technique and miniature specimens to be compared with results from conventional testing, using visual measurement and large CT specimens, Figure 2.1.5. Good agreement was obtained between the two techniques. Data from both tests linearly extends into the region of interest to reactor first wall design, the low da/dN versus AK region.

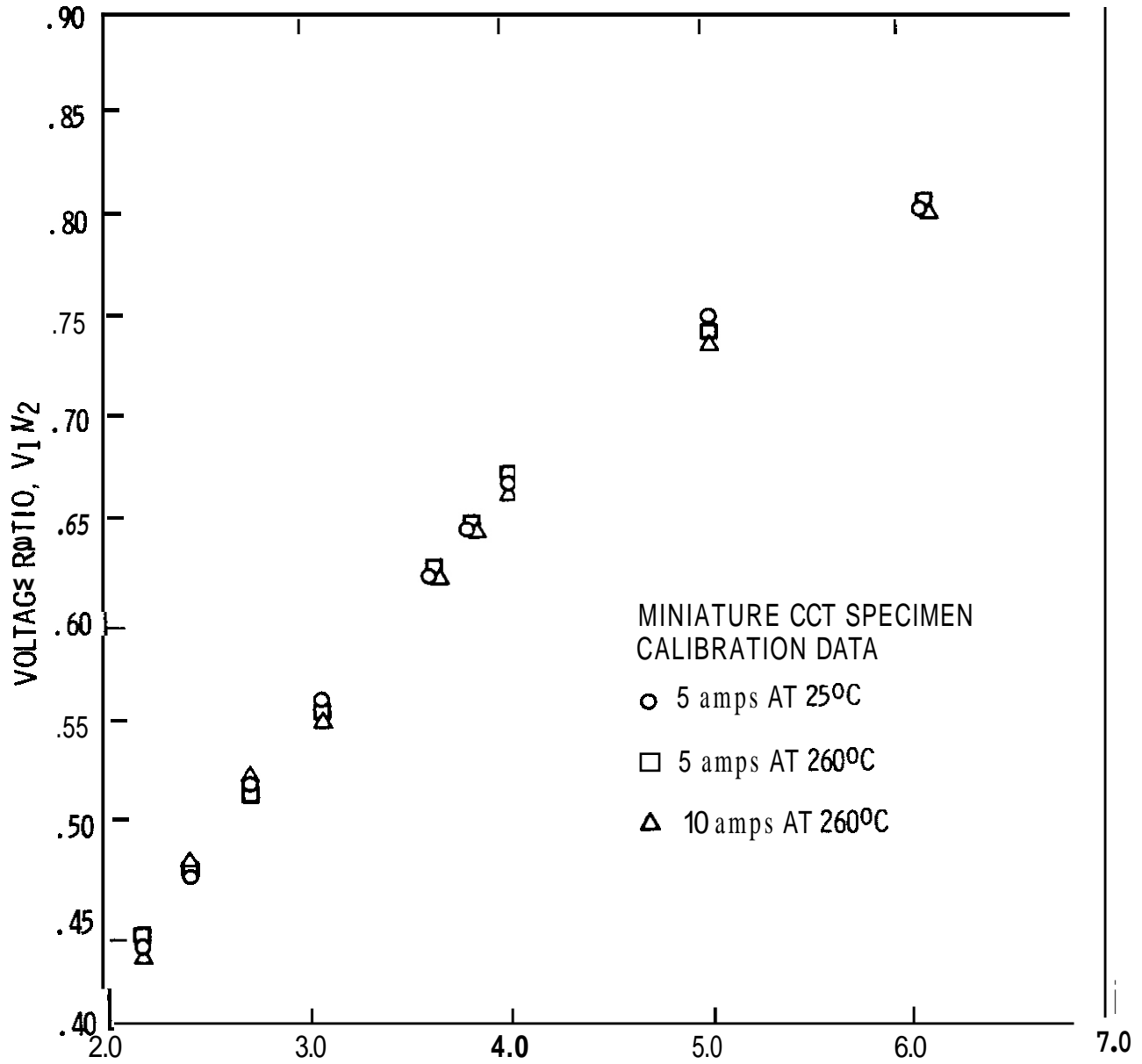


Figure 2.1.3 Miniature Specimen Calibration Curve

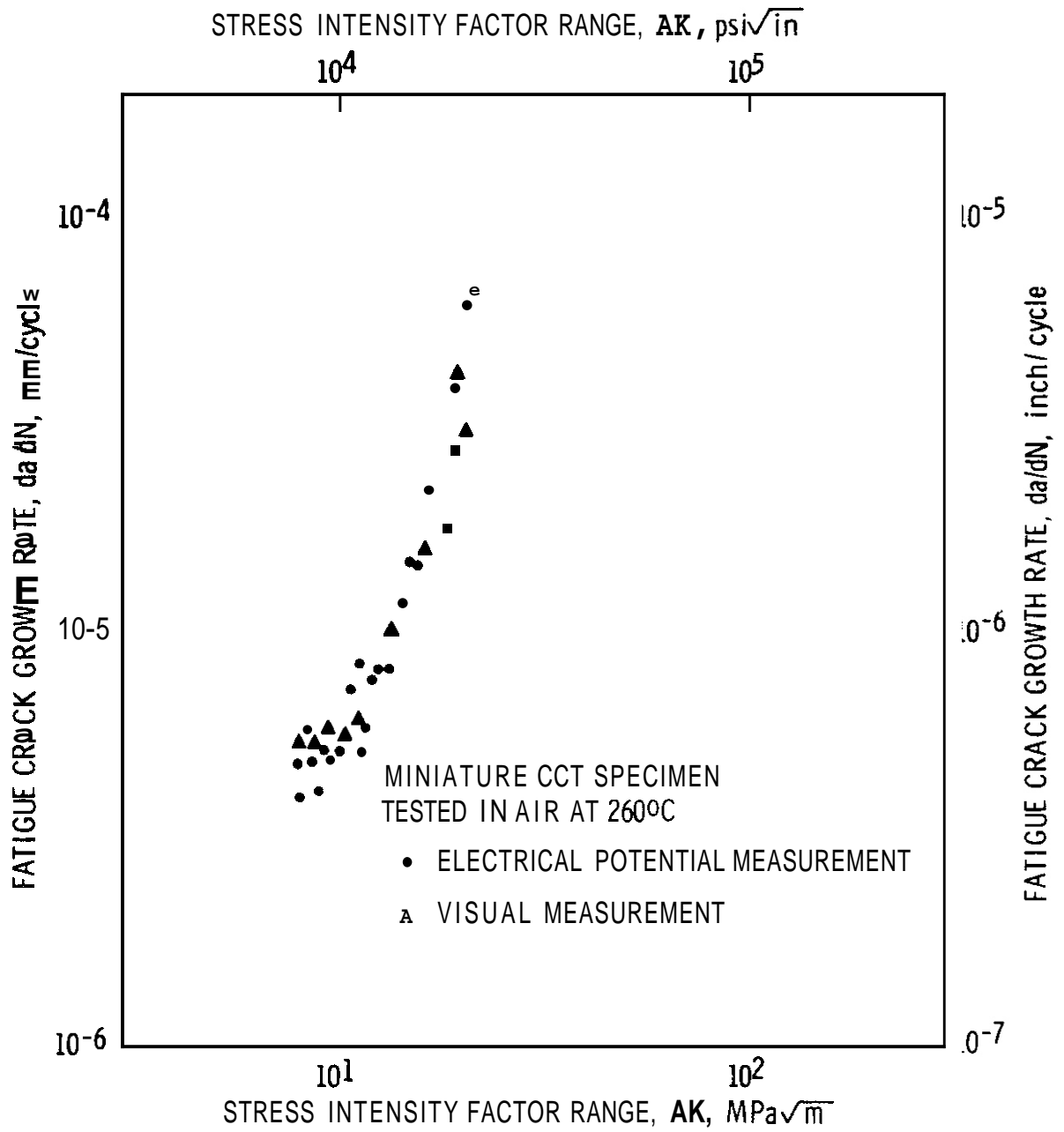
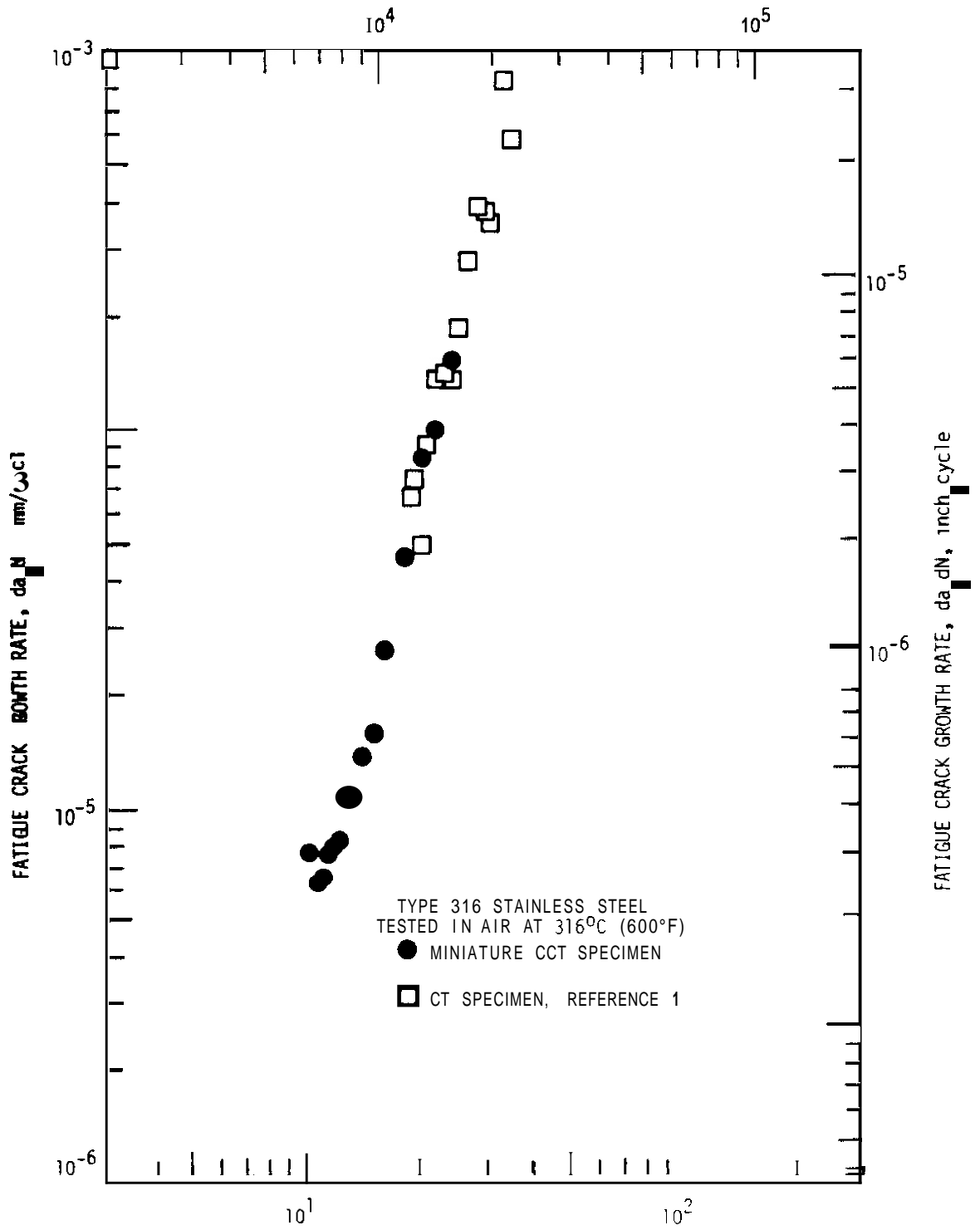


Figure 2.1.4 Comparison of Elevated Temperature Fatigue Crack Growth Rates Determined by Visual and Electrical Potential Methods



2.1.5 Conclusion

The electrical potential technique of measuring crack growth rates in miniature CCT specimens has been adapted to elevated temperature testing. The accuracy of the data has been confirmed by comparison to conventional techniques.

2.1.6. Future Work

Baseline data on non-irradiated candidate alloys can now be generated. Fatigue crack growth testing of these alloys will be initiated using the miniature specimen technology.

2.1.7 References

1. L. A. James, "The Effect of Elevated Temperature Upon the Fatigue-Crack Propagation Behavior of Two Austenitic Stainless Steels," *Mechanical Behavior of Materials, Vol. 111*, pp. 341-352, Society of Materials Science, Japan, 1972.
2. J. L. Straalsund and D. A. Mervyn, "Adaptation of an Electrical Potential Technique to Measure Fatigue Crack Growth," *Alloy Development for Irradiation Performance Quarterly Progress Report for Period Ending December 31, 1978*.
3. L. A. James, R. E. Bauer, and J. L. Straalsund, "Development of Small Fatigue-Crack Growth Specimens for In-Reactor and Post-irradiation Testing," *Alloy Development for Irradiation Performance Quarterly Progress Report for Period Ending June 30, 1978*.
4. R. O. Ritchie, G. G. Garrett, and J. F. Knott, "Crack-Growth Monitoring: Optimization of the Electrical Potential Technique Using an Analogue Method," *Int. Journ. of Fracture Mech.*, pp. 462-467, 7(1971)
5. D. M. Gilby and S. Pearson, "Measurement of the Length of a Central or Edge Crack in a Sheet of Metal By an Electrical Resistance Method," *Royal Aircraft Establishment Technical Report No. 66402*, Dec. '66.
6. R. O. Ritchie and K. J. Bathe, "On the Calibration of the Electrical Potential Technique for Monitoring Crack Growth Using Finite Elements Methods," *International Journal of Fracture, Vol. 15*, No. 1, Feb. 1979.

7. W. Chen and H. W. Liu, "Fatigue Crack Growth at Elevated Temperature 316 Stainless Steel and H-13 Steel," *National Aeronautics and Space Administration Technical Report. NASA Grant No. NGR 33-022-25F.*

2.2 STATUS OF AN IN-REACTOR FATIGUE CRACK PROPAGATION EXPERIMENT -

A. M. Ermi (Hanford Engineering Development Laboratory)

2.2.1 ADIP Task

Task **I.B.1**, Fatigue Crack Growth in Austenitic Alloys (Path A).

2.2.2 Objectives

An apparatus is being developed to perform in-reactor fatigue crack propagation tests on the Path A Reference Alloy. Effects of dynamic irradiation on crack growth behavior will be evaluated by comparing the results with those of unirradiated and postirradiated tests.

2.2.3 Summary

The design of an in-reactor fatigue machine capable of performing tension/tension cycling on a chain of center-cracked-tension specimens in the ORR is nearing completion. A tentative test matrix has been established using the Path A Reference Alloy, 20% cold work 316 stainless steel.

2.2.4 Progress and Status

2.2.4.1 Introduction

The fatigue crack propagation (FCP) behavior of candidate first wall fusion reactor materials must be well understood since crack growth may be a limiting criterion governing fusion reactor lifetimes. To date, all studies of irradiation effects on FCP have been performed on materials irradiated in the unstressed condition, then tested out of reactor. No dynamic irradiation FCP data exists.

Experiments on postirradiated austenitic stainless steels, using either the thermal Advanced Test Reactor¹ or the fast reactor, the EBR-II,¹⁻⁷ have produced mixed results. In general, when the irradiation and test temperature are nearly the same, effects of irradiation are minimal.⁸ However, none of these studies have investigated the effects of irradiation at very small crack growth rates, where microstructure has been observed to have large influences on FCP.⁹

Further interest in a dynamic irradiation FCP experiment was prompted by results of in-reactor versus postirradiated creep tests on austenitic stainless steels.^{10,11} The enhanced creep rupture lives found in those specimens which were stressed during dynamic irradiation was attributed to vast differences in crack growth characteristics.

2.2.4.2 In-Reactor Fatigue Machine

A pneumatically actuated fatigue machine which will perform elevated temperature FCP tests in the ORR (Experiment MFE-5) is in its final stages of design. A schematic illustrating the basic concepts is shown in Fig. 2.2.1.

Miniature center-cracked-tension (CCT) specimens, developed specifically for in-reactor testing,¹² are linked together forming a specimen chain. The bottom of the chain is connected to a rigid specimen support tube, while the top is connected to a bellows. Sodium surrounds the specimens in the core region, while helium at a constant pressure fills the chamber above the sodium. When the pressure in the bellows is cycled with helium, the bellows expands and contracts, providing a cyclic load to the specimen chain. The chamber pressure and the bellows pressure extremes and flow rates are adjustable to provide the desired load range and waveform.

The load will be monitored by two strain gauges welded to each side of the necked portion of the connecting rod. (This section is actually about three feet above the top of the reactor core.) The information from these gauges will be used to make necessary adjustments to the pressures and flow rates.

Irradiation temperature will be controlled by flowing a mixture of helium and neon through a contoured gap between the primary and secondary containment walls. The gas gap will be separated into three independently controlled zones, giving the versatile control necessary to maintain a flat temperature profile despite uncertainties in the gamma heating profile and any time-dependent shifts which may occur in the profile during the reactor cycle. Thermocouples at each specimen and near the strain gauges will continuously monitor the temperature.

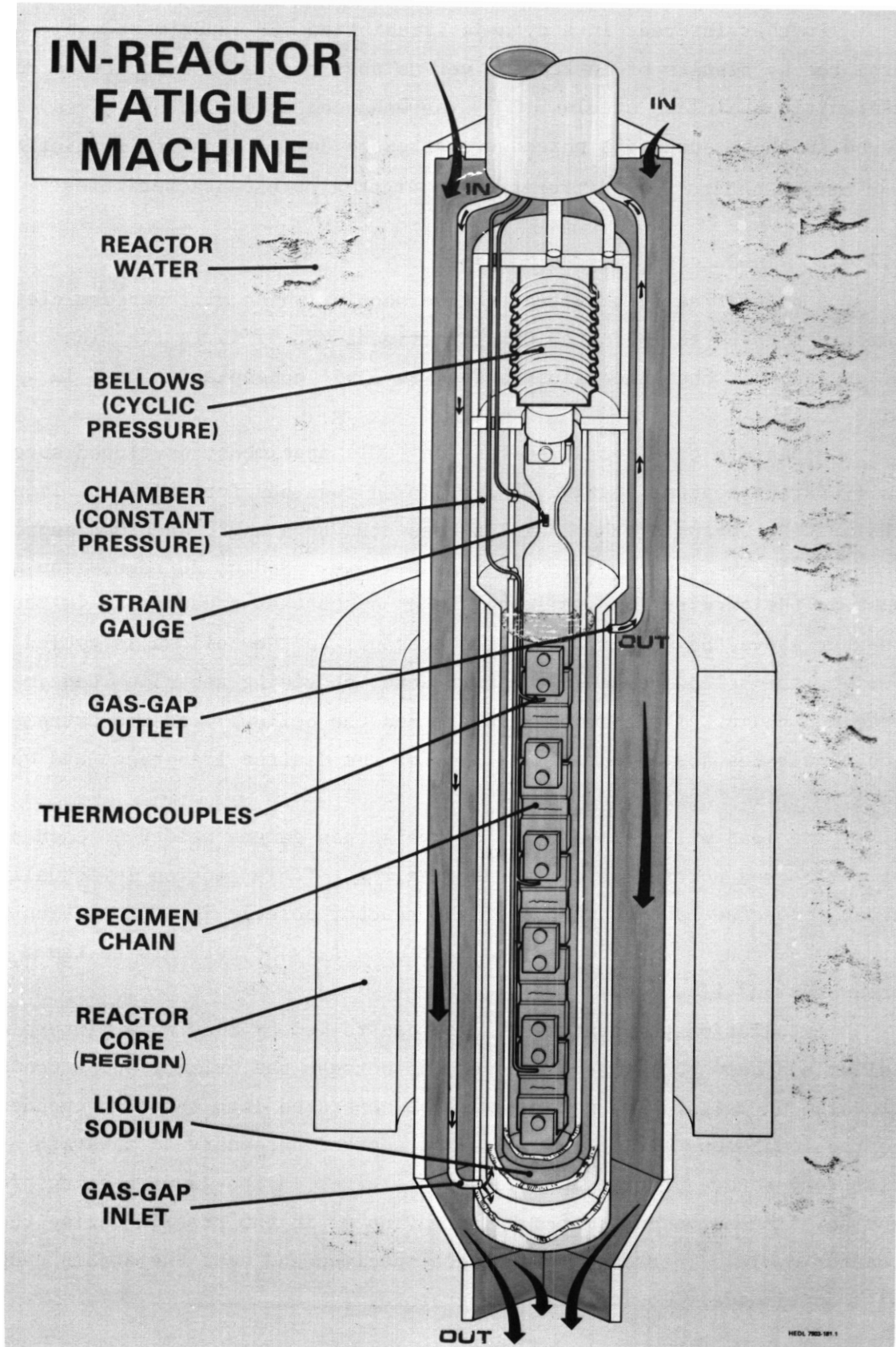


Fig. 2.2.1 Schematic of the In-Reactor Fatigue Machine.

2.2.4.3 Test Matrix

The experiment will be conducted at 425°C in sodium at a frequency of 1 cycle/min. The complete test matrix is listed in Table 2.2.1, while specific details are discussed below.

Irradiation will occur in the ORR, taking advantage of the mixed spectrum and the thermal neutron-nickel two-step reaction, resulting in a He/dpa ratio similar to that expected in a fusion reactor.

Table 2.2.1 In-Reactor Fatigue Crack
Propagation Experiment Test Matrix

Material:	20% cold worked 316 Path A Reference Alloy
Test Reactor:	ORR, experimental location C-7
Temperature:	425°C
Environment:	Sodium
Frequency:	1 cycle/minute
Waveform:	Sawtooth
Stress Ratio:	Min. Load/Max. Load, R=0.05
Stress Intensity:	Load and crack length combinations yielding AK values corresponding to crack growth rates $\sim 10^{-6}$ to 10^{-5} mm/cycle ($\sim 10^{-7}$ to 10^{-6} in/cycle); initial crack lengths and core positions of the eight specimens TBD.
Duration of Test:	Up to six months.

The specimen chain will consist of eight specimens, precracked to five different crack lengths; one crack length will be duplicated and another triplicated. Previous FCP data on stainless steels has indicated that one minute hold times do not effect crack growth in air at 425°C,⁴ and that growth rates in sodium at 425°C are approximately the same as that in air at room temperature.¹³ Consequently, the initial crack lengths for the in-reactor experiment will be based primarily on room temperature

experiments in air on unirradiated specimen chains. These tests will be conducted on both conventional test machines and a prototypic fatigue machine.

In addition to room temperature tests in air, experiments at other temperatures and in other environments will be carried out. Since sodium will not be used in any of these experiments, the crack lengths for each specimen in the chains can be continuously monitored using an electrical potential method,¹⁴ as opposed to the in-reactor test in which only the initial and final crack lengths will be measured.

The duration of the experiment will be determined by the specimen with the largest precrack, the test terminating after a predetermined number of cycles, or after gross yielding or complete separation of a specimen, whichever is first. At this time, the final crack lengths will be measured and the results compared with those of an ex-reactor test conducted at HEDL. The HEDL test will be run on the prototype under the identical test conditions, including the sodium environment. It will parallel the ORR experiment, trailing it by a few days. This will allow for communication between the labs to assure that the HEDL test duplicates the ORR test in every way. The end result is that one-to-one comparisons between dynamically irradiated and unirradiated specimens anywhere in the chain can be made.

Plans also include placement of miniature CCT specimen inserts at positions along the chain of the in-reactor experiment. These inserts will later be welded to the CCT grips, and postirradiated tests performed under conditions similar to the in-reactor and ex-reactor experiments.

2.2.5 Future Work

Fabrication of a prototypic fatigue machine to be tested at HEDL is underway. The prototype will be used in the establishment of the data base and serve as a design basis for the final in-reactor fatigue machine. Specimen chains will also be tested on conventional MTS machines to complement the data base.

2.2.6 References

1. P. Shahinian, H. E. Watson and H. H. Smith, "Effect of Neutron Irradiation on Fatigue Crack Propagation in Types 304 and 316 Stainless Steels at High Temperatures," *ASTM STP-529*, pp. 493-508, 1973.
2. L. A. James and R. L. Knecht, "Fatigue Crack Propagation in Fast Neutron Irradiated Types 304 and 316 Stainless Steels," *Nuclear Technology, Vol. 19*, pp. 148-155, Sept. 1973.
3. P. Shahinian, "Fatigue Crack Propagation in Fast Neutron Irradiated Stainless Steels and Welds," *ASTM STP-570*, pp. 191-204, 1975.
4. D. J. Michel, H. H. Smith and H. E. Watson, "Effect of Hold Time on Elevated Temperature Fatigue Crack Propagation in Fast Neutron Irradiated and Unirradiated Type 316 Stainless Steel," *Structural Materials for Service at Elevated Temperatures in Nuclear Power Generation, ASME*, pp. 167-190, 1975.
5. L. A. James, "The Effect of Fast Neutron Irradiation Upon the Fatigue Crack Propagation Behavior of Two Austenitic Stainless Steels," *Journal of Nuclear Materials, Vol. 59*, pp. 183-191, 1976.
6. D. J. Michel and H. H. Smith, "Fatigue Crack Propagation in Neutron Irradiated Type 304 and Type 308 Stainless Steel Plate and Weld Materials," *Journal of Nuclear Materials, Vol. 71*, pp. 173-179, 1977.
7. D. J. Michel and H. H. Smith, "Effect of Neutron Irradiation on Fatigue Crack Propagation in Type 316 Stainless Steel at 649°C," *NRL Memorandum Report 3936*, March 14, 1979.
8. L. A. James, "Effects of Irradiation and Thermal Aging Upon Fatigue Crack Growth Behavior of Reactor Pressure Boundary Materials," presented at the *IAEA Technical Committee Meeting*, Innsbruck, Austria, Nov. 20-21, 1978; HEDL-SA-1663.
9. R. O. Ritchie, "Influence of Microstructure on Near-Threshold Fatigue Crack Propagation in Ultra-High Strength Steel," *Metal Science*, pp. 368-381, Aug./Sept., 1977.

10. E. R. Gilbert, A. J. Lovell and B. A. Chin, "High Temperature In-Reactor Creep of 20% Cold Worked FTR Cladding," presented at the *9th ASTM International Symposium, Effects of Radiation on Structural Materials*, Dec. 1977; HEDL-SA-1402 A.
11. E. R. Gilbert and B. A. Chin, "In-Reactor Creep Measurements," presented at the *Annual Meeting of American Nuclear Society Special Session on In-Reactor Creep of Structural Materials*, San Diego, June 1978; HEDL-SA-1403-5.
12. L. A. James, J. L. Straalsund and R. E. Bauer, "Optimization of Fatigue Crack Growth Testing for First Wall Materials Development Evaluations," presented at the *First Topical Meeting on Fusion Reactor Materials*, Miami Beach, Jan. 29-31, 1979; HEDL-SA-1621.
13. L. A. James and R. L. Knecht, "Fatigue Crack Propagation Behavior of Type 304 Stainless Steel in a Liquid Sodium Environment, *Met. Trans., Vol. 6A*, pp. 109-116, Jan. 1975.
14. J. L. Straalsund and D. A. Mervyn, "Adaptation of an Electrical Potential Technique to Measure Fatigue Crack Growth," *ADIP Quarterly Progress Report*, Dec. 31, 1978, DOE/ET-0058/4, pp. 4-9.

2.3 NEUTRONIC DESIGN OF SPECTRAL TAILORING EXPERIMENTS — T. A. Gabriel, R. A. Lillie, and B. L. Bishop (ORNL)

2.3.1 ADIP Task

ADIP Task I.A.2, Define Test Matrices and Test Procedures.

2.3.2 Objective

The helium and displacement rates expected near or at the first wall in fusion reactors for stainless steel and nickel-base alloys can be reproduced in fission reactors by varying the thermal-to-fast neutron flux ratio. The helium production will be dominated by the thermal flux and the fast flux will determine the displacement rate. The objective of this work is to determine the amount of variation necessary and to design core pieces for the Oak Ridge Research Reactor (ORR) that will produce the needed changes.

2.3.3 Summary

We have calculated the effect of a tantalum core piece in the ORR on the thermal neutron flux and displacement rate in an enclosed experimental capsule. The large thermal capture cross section of tantalum [about $2.0 \times 10^{-27} \text{ m}^2$ (20 b)] reduces not only the thermal flux but also the displacement rate in the experimental capsule as a result of localized reduction in the number of fissions. This reduction in displacement rate can be partly offset by increasing the fuel loading in adjacent core pieces.

2.3.4 Progress and Status

We have made four VENTURE calculations to determine the effect of a tantalum core piece on the thermal neutron flux and displacement rate in an enclosed experimental capsule. The ORR core configuration used in the first three calculations is shown in Fig. 2.3.1. The tantalum core piece and experimental capsule are located in the C-3 position. The molar composition of the core piece surrounding the experimental capsule for three of the calculations is as follows: (1) 98% Al, 2% H₂O; (2) 50% Ta, 48% Al, 2% H₂O; and (3) 98% Ta, 0% Al, 2% H₂O.

A-1	A-2	A-3	A-4	A-5	A-6	A-7	A-8	A-9
Be	Be	210	180	195	165	225	Be	Be
B-1	B-2	B-3	B-4 SR	B-5	B-6 SR	B-7	B-8	B-9
Be	240	185	110	150	110	165	240	Be
C-1	C-2	C-3	C-4	C-5	C-6	C-7	C-8	C-9
Be	210	Exp	165	135	120	Exp	210	Be
D-1	D-2	D-3	D-4 SR	D-5	D-6 SR	D-7	D-8	D-9
Be	210	155	140	120	140	135	Hyd	Be
E-1	E-2	E-3	E-4	E-5	E-6	E-7	E-8	E-9
Be	195	Exp	150	150	150	Exp	195	Be
F-1	F-2	F-3	F-4	F-5	F-6 SR	F-7	F-8	F-9
Be	225	180	no	240	80	180	225	Be
G-1	G-2	G-3	G-4	G-5	G-6	G-7	G-8	G-9
Be	Be	Be	Be	Be	Be	Be	Be	Be

Fuel Element Loadings in g of ^{235}U .

Be - beryllium element

HT - hydraulic tube

SR - shim rod

Fig. 2.3.1. The ORR Core Configuration Used in the Neutronic Calculations. The calculations were for the C-3 lattice position.

The results of these calculations are shown in Fig. 2.3.2. As can be seen the thermal neutron flux is reduced substantially. The displacement rate is also reduced, but only by about 40%. Since the tantalum core piece is to be used during the later phases of the irradiation experiment, we desire that the thermal flux be reduced while the displacement rate is either increased or at least held to a very moderate decrease. To compensate for this reduction in the displacement rate, the third calculation (98%Ta) was repeated with additional fuel added to the core pieces around C-3: 55 g to B-3, 30 g to B-4, 75 g to C-4, and 85 g to D-3. This additional fuel resulted in about a 10% further decrease in the thermal flux but also yielded a substantial increase of about 20% in the displacement rate.

One reaction that has not been considered in our calculations deals with the production of ^{182}Ta . This isotope is produced in large concentrations during irradiation and has a rather large thermal capture

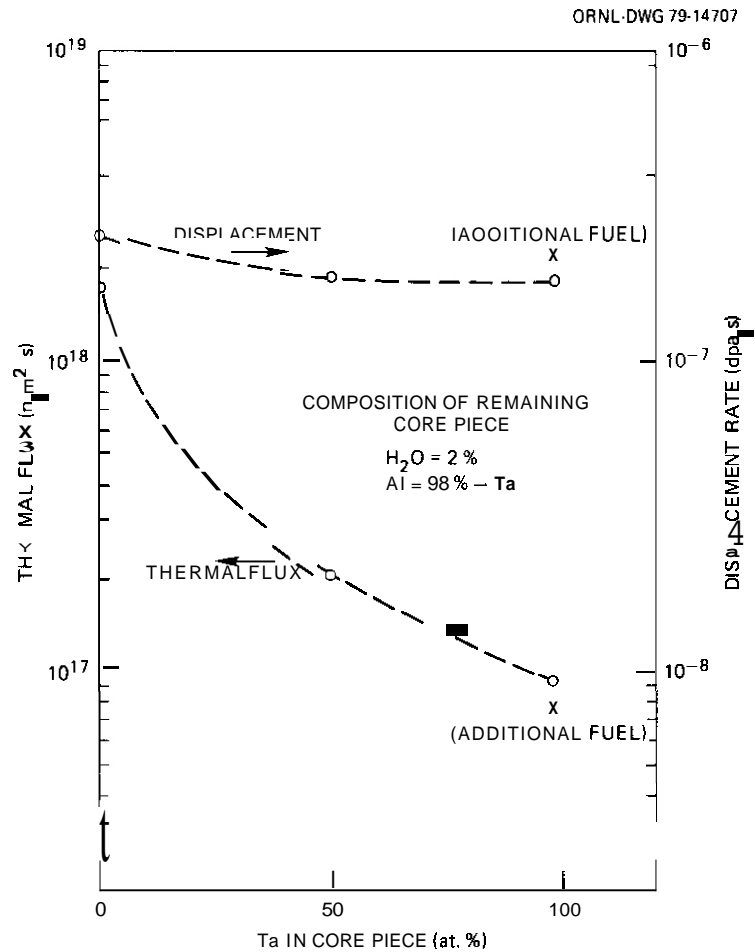


Fig. 2.3.2. Variation of the Displacement Rate and Thermal Flux as Functions of Tantalum Content in the Core Piece. The core piece is located in the C-3 lattice position in the ORR core.

cross section [$\sim 8.0 \times 10^{-25} \text{ m}^2$ ($\sim 8 \times 10^3 \text{ b}$)]. The effect of the production of this element on the thermal flux and displacement rate will be investigated in the future.

2.3.5 Conclusions

We have reduced the thermal neutron flux in an ORR experimental capsule substantially by use of a tantalum core piece. However, to retain a high displacement rate, a large fuel loading must be maintained around the experimental position.

2.4 DESIGN OF IRRADIATION EXPERIMENTS IN ORR USING SPECTRAL TAILORING AND REENCAPSULATION — K. Thoms and M. L. Grossbeck (ORNL)

2.4.1 ADIP Task

ADIP Task I.A.2, Define Test Matrices and Test Procedures.

2.4.2 Objective

The objective of this work is to produce the thermal and mechanical design of experiments for material irradiation in the ORR core. The ORR-MFE-4 experiments will operate with spectral tailoring to control the fast and thermal fluxes and thus the displacement and helium production rates. The capsules are also designed for both discharging specimens and reloading with irradiated specimens several times during the experiment lifetime.

2.4.3 Summary

We have designed and drawn the two experiments ORR-MFE-4A and ORR-MFE-4B. The first experiment will contain specimens at 300 and 400°C, and the second will contain specimens at 500 and 600°C. Parts are being fabricated for a bench test of the experiment, and a gamma heat measuring experiment is awaiting irradiation.

2.4.4 Progress and Status

We will operate two materials irradiation experiments concurrently in the ORR, irradiating material specimens at four different test temperatures. The first experiment, ORR-MFE-4A, will be placed in the E-3 core position and will irradiate specimens at 300 and 400°C. The second experiment, ORR-MFE-4B, will be placed in the E-7 core position and will irradiate specimens at 500 and 600°C. All detail drawings for this series of experiments have been completed and are presently being reviewed.

Parts are presently being fabricated to build a bench test of the in-core section of the proposed design. The two purposes of this test

are to work out the complicated fabrication and assembly requirements of this portion of the experiments and to determine the temperature control capabilities of the experiment design.

We assembled a gamma heat measuring device. However, as a result of the ORR operating schedule, we will not be able to make gamma heat measurements until the week of July 10-15 when the reactor will be shut down for major maintenance and experimental work. At that time we will measure gamma heating rates in the first two core piece designs in the E-3 core position. The E-7 core position cannot be measured at this time because ORK-MFE-2 is in that position. We feel that E-3 and E-7, being symmetrical about the reactor centerline, will have approximately the same gamma heating rates.

3. PATH A ALLOY DEVELOPMENT — AUSTENITIC STAINLESS STEELS

Path A Alloys are those alloys generally known as austenitic stainless steels. The most common U.S. designations are AISI types 304, 316, 321, and 347. Primary considerations for selecting this class of alloys for further development are:

1. state-of-the-art production and fabrication technology;
2. extensive data on the effects of neutron irradiation on properties, which show the potential of these alloys for MFK applications;
3. compatibility with proposed coolants and breeding fluids;
4. evidence that for MFR conditions (He, dpa, temperatures) the properties are sensitive to composition and microstructure — thus showing potential for further development.

The strategy for development of these alloys has two related objectives:

1. to determine for a reference alloy the effects of irradiation on those properties most important to fusion reactor design;
2. to develop a path A alloy that is optimized for fusion reactor applications.

The first objective will provide a data base for near-term reactor design and, most important, guidance as to which properties limit performance of this type alloy. Work on the reference alloy will provide direction for the actual alloy development efforts of the second objective. Type 316 stainless steel in the 20%-cold-worked condition appears to be the best choice as a reference alloy. It is the present reference cladding and duct alloy in the breeder reactor programs, and there are extensive data on the unirradiated mechanical properties, effects of heat treatment on properties, structure, and phase stability, and the effects of fast neutron irradiation on properties. The present technology of austenitic stainless steels, including understanding of the physical and mechanical properties and irradiation response, is such that alloy development efforts can move to optimization for use in fusion reactor applications. A Prime Candidate Alloy (PCA) (Fe-16% Ni-14% Cr-2% Mo-2% Mn-0.5% Si-0.2% Ti-0.05% C) has been selected by the ADIP task group. Efforts will now focus on optimizing the composition and microstructure of the PCA leading toward the selection of OPT-A1 (Program Plan designation of first optimized path A alloy).

3.1 LOW-CYCLE FATIGUE BEHAVIOR OF 20%-COLD-WORKED TYPE 316 STAINLESS STEEL AFTER IRRADIATION IN THE HFIR — M. L. Grossbeck and K. C. Liu (ORNL)

3.1.1 ADIP Task

ADIP Task I.B.5, Stress-Strain Controlled Fatigue of Austenitic Alloys.

3.1.2 Objective

This study evaluates the effects of simultaneous displacement damage and helium production during irradiation on the low-cycle fatigue life of 20%-cold-worked type 316 stainless steel.

3.1.3 Summary

Specimens of 20%-cold-worked type 316 stainless steel were irradiated in the High Flux Isotope Reactor (HFIR) to fluences of 0.85 to 1.9×10^{26} n/m², resulting in displacement levels of 7 to 15 dpa and helium contents of 250 to 860 at. ppm. Fully reversed strain controlled fatigue tests were performed with strain ranges of 0.40 to 2.0%. The specimens were irradiated and tested at 430°C and tested in a vacuum at a pressure below 10^{-4} Pa. The fatigue life was reduced by factors of 3 to 10. We are studying fracture surfaces and will subsequently report the results.

3.1.4 Progress and Status

3.1.4.1 Introduction

Since a tokamak reactor operates in a cyclic mode, thermal stresses will result in fatigue in structural components, especially in the first wall and blanket. There has been limited work on fatigue in irradiated alloys¹ but none on irradiated materials containing irradiation-induced helium. To provide scoping data and to study the effects of irradiation on fatigue behavior, we studied 20%-cold-worked type 316 stainless steel from the MFE reference heat.

3.1.4.2 Experimental Procedure

Hourglass specimens with minimum gage diameters of 3.18 mm (0.125 in.) were irradiated in the HFIR in peripheral target positions, providing both a high rate of displacement damage and rapid helium production from interaction of thermal neutrons with nickel. A helium gas gap controlled the temperature. The experiment was monitored by inclusion of low-melting alloys, as described previously.²

Tests were performed on a servo hydraulic testing system equipped for remote operation.³ Specimens were tested in a vacuum at pressures from 10^{-5} to 10^{-4} Pa. The gage section of the specimen was maintained at $430^{\circ}\text{C} \pm 5^{\circ}\text{C}$, remaining constant within $\pm 1^{\circ}\text{C}$ during the test. Strain was measured at the minimum cross section with a diametral extensometer with ceramic blades and a linear variable differential transformer (LVDT). The diametral signal in turn was converted to an equivalent axial strain through a strain computer for machine control. A fully reversed ramp function providing a strain rate of $4 \times 10^{-3}/\text{s}$ was used. Specimens were cycled to complete separation. We estimated crack initiation from continuous stress plots by determining the point of load drop from cracking.

Following failure, fracture surfaces are studied with a scanning electron microscope (SEM). Results of the fracture studies are incomplete but will be reported subsequently.

3.1.4.3 Results and Discussion

Results of the fatigue tests are tabulated in Table 3.1.1 and plotted in Fig. 3.1.1. Comparison of data from irradiated and unirradiated specimens reveals a reduction in fatigue life by a factor of 3 to 10, with a somewhat broad scatter band for the irradiated data. This is consistent with the data of Beeston and Brinkman,¹ who observed a reduction factor of approximately 2 in fatigue life for irradiated type 316 stainless steel. Their irradiations in EBR-II were to fluences close to our HFIR exposures; however, helium effects are absent or greatly reduced for the EBR-II case.

Table 3.1.1. Results of Fatigue Tests on Unirradiated and Irradiated Specimens of 20%-Cold-Worked Type 316 Stainless Steel

Specimen	Fluence >0.1 MeV (n/m^2)	He (at. ppm)	Total Strain Range (%)	Cycles		Life Before Crack Initiator (%)
				To Failure	To Crack	
G6	0		2.0	2,5511	2,120	91
A96	0		1.5	2,602	2,510	97
G28	0		1.4	8,295	6,9211	83
G35	0		1.2	14,250	14,150	99
A68	0		1.0	28,470	17,100	60
G33	0		1.0	11,1131	10,060	91
G8	0		1.0	20,400	10,1111	99
A57	0		11.71	3,444	1,240	311
G26	0		0.70	59,001	56,580	96
G7	0		0.60	57,668	48,680	84
A56	0		0.50	>293,826		
A39	$0.85 \cdot 10^{26}$	250	1.5	1,272	1,080	85
A23	0.85	250	1.0	1,881	1,300	69
G71	0.85	250	0.50	105,097		
A37	1.2	4411	2.0	1,360	450	33
Ab?	1.2	440	1.0	6,934	6,160	89
A64	1.2	4411	0.70	3,616	2,350	65
A22	1.4	5311	1.5	2,220	1,7611	19
A2	1.4	530	0.50	13,330	7,120	53
A8	1.6	660	0.70	1,940	1,550	80
A	1.9	860	2.0	4RJ	400	83
A6	1.9	860	1.0	4,210	2,900	69
A7	1.9	830	0.50	26,175	7,000	27

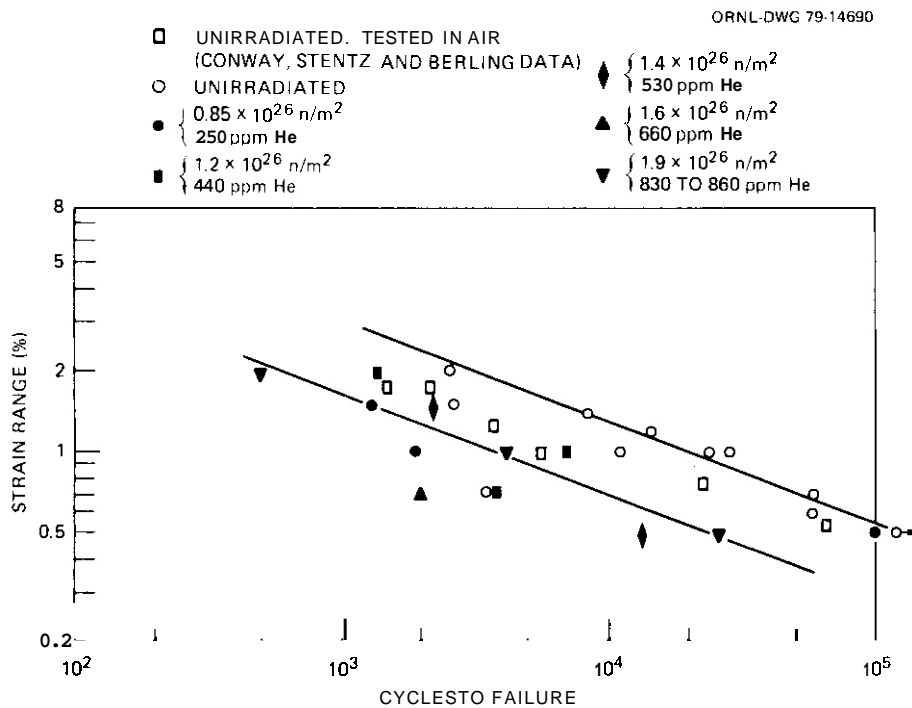


Fig. 3.1.1. Fatigue Life of 20%-Cold-Worked Type 316 Stainless Steel Irradiated at 430°C in the HFIR and Tested at 430°C . Source of data on unirradiated specimens tested in air: V. B. Conway, R. H. Stentz, and J. T. Berling, *Fatigue, Tensile and Relaxation Behavior of Stainless Steels*, TID-26135 (1975) p. 39.

Results of fatigue tests performed by Conway, Stentz, and Berling⁴ in air on unirradiated annealed type 316 stainless steel are also plotted in Fig. 3.1.1. A slightly shorter fatigue life is observed when compared with the vacuum data from the present study. Our limited amount of air environment data³ from tests using the same miniature specimens as for the irradiations shows rather good agreement with the Conway et al. data. Although differences in composition, microstructure, and specimen size are important, we believe the difference in test environment to be the major reason for the variance in data shown in Fig. 3.1.1.

To evaluate the effects of irradiation on fatigue life, the cycles to failure were plotted as a function of fluence in Fig. 3.1.2. The reason for the large scatter band for the irradiated data in Fig. 3.1.1 now becomes evident: a well-defined fluence dependence, as a function of strain, becomes evident.

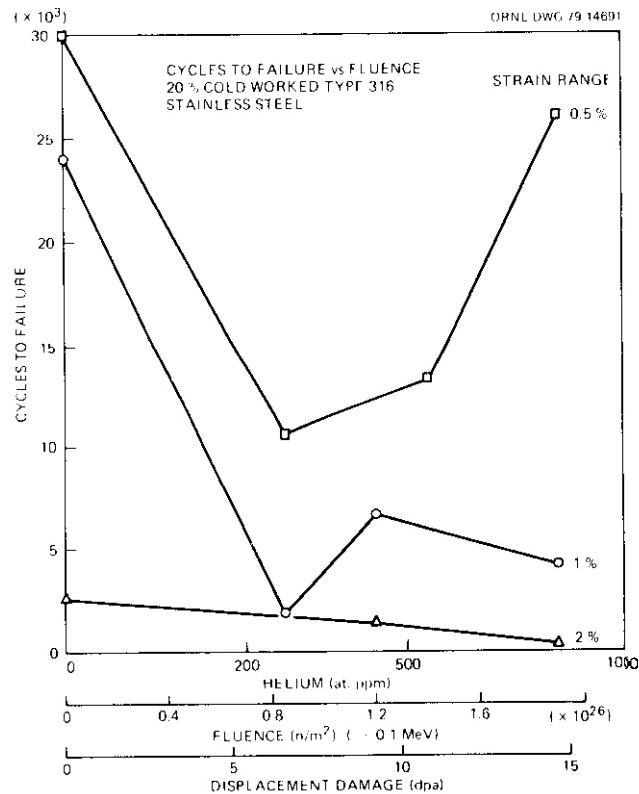


Fig. 3.1.2. Cycles to Failure as a Function of Fluence, Displacement Rate, and Helium Content for Irradiated, 20%-Cold-Worked Type 316 Stainless Steel Tested in Vacuum at Specified Strain Ranges.

For 2% strain range fatigue life decreases monotonically, resulting in a linear plot. Since ductility is the major factor determining fatigue life at high strains, irradiation hardening would be expected to account for the greater reduction in life of the irradiated material compared with that of unirradiated material. However, although ductility decreases initially, it appears to level off at a fluence of $1.6 \times 10^{26} \text{ n/m}^2$.⁵ Therefore, continued reduction must result from a more complex interaction. Higher fluence data are required to determine if the reduction in life continues.

At a strain range of 0.5%, fatigue life passes through a minimum with increasing fluence. A possible explanation is that fatigue life initially drops as a result of irradiation hardening and embrittlement. However, once helium bubbles are formed, they impede dislocation motion at these stress levels, resulting in a slower progression of fatigue damage. Since cavities containing helium grow with increasing fluence, they will lose their effectiveness at higher fluence levels because they will be less effective obstacles to dislocation motion. The trend of increasing fatigue life with increasing fluence exhibited by the 0.5% curve in Fig. 3.1.2 would then not be expected to continue.

The behavior of the material cycled at 1% total strain range is intermediate between the other two curves and will not be discussed.

From Table 3.1.1 the fraction of the specimen's life before crack initiation is larger for unirradiated material than for irradiated material. For unirradiated specimens 84% of the cyclic life is spent before crack initiation in contrast to 67% spent for irradiated specimens. We feel that this result is sufficiently large to be significant. The result is not unexpected since the effect of dislocation pinning is most significant in microstructure development leading to crack initiation.

3.1.4.4 Conclusions

The effects of helium and the increase in cyclic life with increasing fluence will be better understood when fractography and transmission electron microscopy studies are complete. In the interim

we can only assume that fatigue life is reduced by a factor of 3 to 10 by irradiation to a fluence of 1.9×10^{26} n/m² as shown in Fig. 3.1.1. When more data become available, an equation relating fatigue life, strain range, and fluence will be developed.

3.1.5 References

1. J. M. Beeston and C. R. Brinkman, "Axial Fatigue of Irradiated Stainless Steels Tested at Elevated Temperatures," pp. 419–50 in *Irradiation Effects on Structural Alloys for Nuclear Reactor Applications*, ASTM STP 484, American Society for Testing and Materials, Philadelphia, Pa., 1970.
2. M. L. Grossbeck and M. J. Kania, "HFIR Irradiation of Hourglass Fatigue Specimens," *ADIP Program Quart. Prog. Rep. May 1979*, DOE/ET/0058/2, pp. 20–35,
3. K. C. Liu and M. L. Grossbeck, "Status of Fatigue Testing Facility," *ADIP Program Quart. Prog. Rep. May 1979*, DOE/ET/0058/2, pp. 54–59.
4. J. B. Conway, R. H. Stentz, and J. T. Berling, *Fatigue, Tensile, and Relaxation Behavior of Stainless Steels*, TID-26135 (1975) p. 39.
5. M. L. Grossbeck and P. J. Maziasz, "Tensile Properties of Type 316 Stainless Steel Irradiated in a Simulated Fusion Reactor Environment," paper presented at First Topical Meeting on Fusion Reactor Materials, Miami Beach, Fla., Jan. 1979.
6. Personal communication, P. J. Maziasz, Oak Ridge National Laboratory, July 1979.

3.2 MICROSTRUCTURAL DESIGN FOR FUSION FIRST-WALL APPLICATIONS AND RECOMMENDATIONS FOR THERMAL-MECHANICAL PREIRRADIATION TREATMENTS - P. J. Maziasz (ORNL)

3.2.1 ADIP Tasks

ADIP Task I.A.4, Fabrication Analysis; and I.C.1, Microstructural Stability.

3.2.2 Objective

The objective of this work is to design preirradiation microstructures that will improve the properties of the Prime Candidate Alloy (PCA) during irradiation. We will use information on irradiation response of austenitic alloys from previous work to determine optimum microstructures and to seek thermal-mechanical treatments that will produce these microstructures.

3.2.3 Summary

Previous work [including High Flux Isotope Reactor (HFIR) tests] on the effects of helium in metals indicates that the chances of maintaining good mechanical response in a fusion reactor depend on keeping helium away from the grain boundaries and trapping it intragranularly. Swelling from helium bubble formation is inevitable, but the finest helium distribution will minimize swelling. We propose a matrix of desirable preirradiation microstructures for the PCA based upon responses of type 316 stainless steel or type 316 modified with titanium to HFIR irradiation. Desirable microstructures result from a combination of grain boundary precipitation, cold work, and distribution of titanium-rich MC. We also discuss thermal-mechanical treatments to produce these microstructures. Further work includes completing the fabrication procedures on which microstructural homogeneity and control intimately depend.

3.2.4 Introduction

Considerable data exist on the mechanical properties, microstructures, and swelling of solution-annealed (1 h at 1050°C) and 20%-cold-worked types 316 and 316 modified-with-titanium (**0.23 wt % Ti**) austenitic stainless

steel after irradiation in the HFIR at temperatures of 280 to 800°C.¹⁻⁹ No true fusion environments currently exist, and all simulation environments have both advantages and drawbacks. Use of HFIR irradiation is the only way to reach fusion-level helium production with simultaneous displacement damage. Even though the He/dpa ratio is higher in the HFIR than expected in fusion, various compositions of steel and their corresponding microstructures can be compared after HFIR irradiation to provide correlations between the resulting microstructure and the swelling and mechanical properties of the steel. These correlations give information on properties that provides a basis for preirradiation microstructural design for optimal helium accommodation.

Experimental observations of the effects of helium on the properties and microstructures of metals¹⁰⁻¹⁴ correlate quite well with theoretical calculations and concepts.^{15,16} Cavities formed by thermally aging an initial distribution of helium exhibit the following characteristics:

1. the cavities formed are equilibrium helium bubbles, nearly always located at dislocations or grain boundaries;
2. grain boundary cavities are larger than matrix cavities, and a cavity denuded zone is adjacent to the grain boundary;
3. cavities are never observed to shrink but only grow or coalesce;
4. the number density and size distribution are relatively temperature insensitive.

Cavities in HFIR irradiated type 316 stainless steel behave like bath bubbles and voids.³ The cavities are nearly always equilibrium bubbles. Though they behave like bubbles with respect to grain boundaries and dislocations, their number density decreases and size increases with increasing temperature like voids. Cavities form at both higher (800°C) and lower (280°C) temperatures and increase in number for a given temperature and fluence than voids. In many cases void formation can be suppressed and swelling can be eliminated. However, helium bubbles always form, causing some swelling.

After HFIR irradiation that produced 200 to 4000 at. ppm He,⁶⁻⁸ the mechanical behavior of type 316 stainless steel is at best similar to that of high-temperature helium embrittlement after irradiation that

produces 1 to 10 at. ppm He.^{17,18} High-temperature helium embrittlement is generally characterized by intragranular failure at low ductility. This behavior is attributed to helium weakening the grain boundaries and simultaneously strengthening the grains. After high fluence HFIR irradiation, grain boundary cavitation always coincides with intergranular failure at ductilities of 0 to 1.0% with equal total and uniform elongation. The best mechanical results after HFIR irradiation correlate microstructurally with:

1. intragranular trapping of helium in small cavities at the interface of titanium-rich MC precipitate particles,⁶
2. intragranular trapping of helium in small cavities along dislocation lines,³
3. prevention of the formation of large grain boundary cavities by precipitation of $M_{23}C_6$ and/or eta phase at the grain boundary.³⁻⁶

Combinations of these microstructural features resulted in ductilities as high as 4 to 6% and in some cases with little degradation of the unirradiated properties. This behavior is consistent with the following proposals for preventing helium embrittlement in the microstructure:

1. form blocky precipitate particles at the grain boundaries,¹⁷ and
2. trap helium intragranularly and keep it from accumulating at the grain boundaries.¹⁸

In most cases after HFIR irradiation intragranular accommodation of helium, either in small cavities at dislocations or at titanium-rich MC particle interfaces, and elimination of large grain boundary cavities also gives the lowest swelling. With proper fabrication these microstructural features can be combined¹⁹ to provide the basis for designing preirradiation microstructures that can control helium distribution more effectively than microstructures with "free" precipitation behavior (such as those of simple solution-annealed or cold-worked material).

3.2.5 Microstructural Design

Our criteria for selecting preirradiation microstructures are based on the following microstructural features that produce good mechanical behavior, as discussed above:

1. prevent grain boundary cavity formation;
2. trap helium intragranularly;
3. achieve the finest distribution of helium possible;
4. prevent uncontrolled precipitation of Laves, $M_{23}C_6$, eta, gamma-prime, chi, or sigma phases;^{4,5} and
5. prevent recrystallization of cold-worked structure.

Many of these effects are achieved to some degree in type 316 modified with titanium and result from the precipitation of titanium-rich MC particles, which may be the most powerful helium traps in austenitic stainless steel. The Path A PCA, which contains about 0.25 wt % Ti, behaves like type 316 modified with 0.23 wt % Ti.¹⁸ We have assumed that the irradiated response of the Path A PCA will be like that of type 316 modified with titanium, particularly with respect to MC precipitation. Consequently we have based several proposed microstructures and recommended thermal-mechanical treatments for the PCA on data from type 316 modified with titanium as a first order approximation.

The suggested preirradiation microstructures are as follows:

- A. simple microstructure with "free" precipitation resulting from:
 1. solution annealing,
 2. 5 to 10% cold working, or
 3. 20 to 25% cold working.
- B. microstructures with intragranular titanium-rich MC, no grain boundary precipitation, and an MC precipitate particle density of:
 1. 1×10^{20} particles/ m^3 ,
 2. 1×10^{21} particles/ m^3 , or
 3. 1×10^{22} particles/ m^3 ,
- C. microstructures with intragranular titanium-rich MC, grain boundary $M_{23}C_6$ and/or eta phase, and an MC precipitate particle density of:
 1. 1×10^{20} particles/ m^3 ,
 2. 1×10^{21} particles/ m^3 , or
 3. 1×10^{22} particles/ m^3 .
- D. microstructures with intragranular and grain boundary titanium-rich MC and an intragranular MC precipitate particle density of:
 1. 1×10^{20} particles/ m^3 ,
 2. 1×10^{21} particles/ m^3 , or
 3. 1×10^{22} particles/ m^3 .

The simple preirradiation microstructures resulting from treatments A1, A2, and A3 are included because these microstructures have very good properties at some temperatures after intermediate fluence irradiation.⁷⁻⁹ Furthermore, we are using them as a baseline for comparing the effects of other treatments. Solution-annealed type 316 modified-with-titanium stainless steel irradiated in the HFIR at 600°C contained a precipitate particle density of about 1×10^{20} particles/m³. The region around each precipitate was completely denuded of cavities. The denuded zones at that density just overlap to protect the entire matrix. Therefore, 1×10^{20} particles/m³ is the minimum necessary precipitate density. The presence of titanium-rich MC particles results in the accommodation of helium in small cavities at the particle interface. Thus making the MC distribution finer will provide more interface for a given precipitate particle volume fraction. The upper distribution limit appears to be 1 to 2×10^{22} particles/m³, which results from thermal aging²⁰ or HFIR irradiation' of 20%-cold-worked type 316 modified with titanium. This precipitate particle density can prevent recrystallization by locking the dislocation structure but also increases unirradiated strength and decreases ductility. We have selected an intermediate precipitate particle density of 1×10^{21} particles/m³ in an attempt to optimize helium accommodation and increase unirradiated ductility. Furthermore, cascade dissolution of small (about 3.0 nm or less) precipitate particles²¹ may not allow the highest number density of fine precipitates to persist at all irradiation conditions.

Microstructures B, C, and D vary in intragranular titanium-rich MC particle density and in the preirradiation condition of the grain boundary. The mechanical properties appear most sensitive to grain boundary condition. It appears desirable that the microstructure contain some distribution of a blocky, grain boundary phase such as M₂₃C₆ or eta phase (microstructure C) before irradiation. Grain boundary precipitation forms at some temperatures during HFIR irradiation. Therefore, comparison of microstructure B with that of C should show how the grain boundary component of the microstructure affects the accommodation of helium relative to a fixed matrix accommodation. Microstructure D replaces M₂₃C₆

and/or eta phase with titanium-rich MC particles. Irradiation of all the above the microstructures at various temperatures and fluences should indicate the advantages and feasibility of varying preirradiation microstructures for given alloy compositions.

3.2.6 Thermal-Mechanical Treatments

The recommended microstructures can be achieved by fabricating materials without precipitating titanium-rich MC particles inhomogeneously. The methods for producing "simple" A microstructures from such material are straightforward. For B, C, and D microstructures, precipitate particle densities 1 and 3 should result from aging at temperatures between 650 and 750°C.^{20,22} The MC precipitate particle density seems most sensitive to initial dislocation density if recrystallization does not occur. Intermediate precipitate density 2 should be achievable by either lightly cold working the material or going to a higher temperature than used for the solution-annealed material, A1. Grain boundary precipitation of $M_{23}C_6$ and/or eta phase usually occurs with the MC precipitation in 20%-cold-worked material at 650 to 750°C. We are now investigating times and temperatures that achieve this. It is not clear if precipitation of grain boundary $M_{23}C_6$ and/or eta phase or MC occurs first, and separation of these two is essential in producing B and D microstructures. Determination of the time-temperature-precipitation (TTP) behavior of the Path A PCA for several cold-worked levels should help clarify which phase precipitates first. In producing B microstructures, MC must precipitate before the grain boundary phases. The production of D microstructures will be the most difficult and probably will involve at least two thermal treatments. Grain boundary precipitation of MC-type carbides has occurred under several isolated conditions, but is not the usual precipitation behavior. The fabrication sequence can be manipulated to include a thermal treatment before the final step. Partial recrystallization may also locate MC-type precipitate particles at grain boundaries. Work is in progress to investigate these effects.

3.2.7 Conclusions and Future Work

1. A review of work on helium in metals indicates that the chances of maintaining good mechanical response in a fusion first wall depends on keeping helium away from the grain boundaries and trapping it intragranularly. Swelling is inevitable with helium, but minimum swelling will be realized with the finest distribution of helium bubbles possible.

2. We propose a matrix of desirable preirradiation microstructures for the PCA based upon microstructural features that best accommodate helium as demonstrated in various types 316 or 316 modified-with-titanium stainless steel samples after HFIR irradiation. Desirable microstructures include various combinations of MC precipitation, dislocation density, and grain boundary precipitation that should give better properties than the "free" precipitation of simple preirradiation microstructures. Irradiation of these proposed microstructures will test the extent to which preirradiation microstructures can be used to control properties.

3. We discuss the thermal-mechanical treatments to achieve the recommended microstructures. Achieving these microstructures depends intimately upon proper fabrication. In most cases the preirradiation microstructures are either "simple" microstructures or require one-step thermal aging treatments. However, the production of grain boundary titanium-rich MC may require several steps.

Future work will include determining the TTP curves for the Path A PCA in several microstructural conditions and beginning longer term aging to provide a baseline for comparison with reactor irradiated material.

3.2.8 References

1. F. W. Wiffen and E. E. Bloom, "Effect of High Helium Content on Stainless-Steel Swelling," *Nucl. Technol.* 25: 113-23 (January 1975).
2. E. E. Bloom and F. W. Wiffen, "The Effects of Large Concentrations of Helium on the Mechanical Properties of Neutron-Irradiated Stainless Steel," *J. Nucl. Mater.* 58(2): 171-84 (1975).
3. P. J. Maziasz, F. W. Wiffen, and E. E. Bloom, "Swelling and Microstructural Changes in Type 316 Stainless Steel Irradiated under Simulated CTR Conditions," *Radiation Effects and Tritium Technology for Fusion Reactors*, CONF-750989, Vol. I (March 1979) pp. 259-88.

4. P. J. Maziasz, "Precipitation Response of Austenitic Stainless Steel to Simulated Fusion Irradiation," pp. 160-80 in *The Metal Science of Stainless Steels*, (Proc. AIME Symposium) AIME, New York, 1979.
5. P. J. Maziasz, "The Precipitation Response of 20%-Cold-Worked Type 316 Stainless Steel to Simulated Fusion Irradiation," to be published in the *Journal of Nuclear Materials*.
6. P. J. Maziasz and E. E. Bloom, "The Effect of Titanium Addition to Type 316 Stainless Steel Irradiated in a Neutron Environment Producing Simultaneous Helium and Displacement Damage," in preparation.
7. M. L. Grossbeck and P. J. Maziasz, "Tensile Properties of HFIR-Irradiated Types 316 and TiM 316 Stainless Steel at 200 to 1000 at. ppm He," *ADIP Quart. Prog. Rep. July 1978*, DOE/ET-0058/3, pp. 32-49.
8. M. L. Grossbeck and P. J. Maziasz, "Tensile Properties of Type 316 Stainless Steel Irradiated in a Simulated Fusion Reactor Environment," to be published in *Journal of Nuclear Materials*.
9. M. L. Grossbeck and P. J. Maziasz, "The Swelling of 20% Cold Worked Type 316 Stainless Steel Irradiated in HFIR to Helium Levels of 200-3700 at. ppm," *ADIP Quart. Prog. Rep. January-March 1978*, DOE/ET-0058/1, pp. 82-85.
10. B. Russell and I. J. Hastings, "A Preliminary Investigation of Helium Gas Precipitation in Irradiated Copper-Boron Alloys," *J. Nucl. Mater.* 17: 30-36 (1965).
11. J. R. Cost and D. L. Johnson, "Site Occupancy and Bubble Formation of Helium in High Purity Aluminum," *J. Nucl. Mater.* 36: 230-33 (1970).
12. P. Vela and B. Russell, "The Behavior of Helium Gas in Irradiated Copper-Boron Alloys," *J. Nucl. Mater.* 19: 312-26 (1966).
13. P. Vela and B. Russell, "Spontaneous Grain Boundary Swelling in Irradiated Copper-Boron Alloys," *J. Nucl. Mater.* 19: 327-40 (1966).
14. R. S. Barnes and D. J. Mazey, "The Migration and Coalescence of Inert Gas Bubbles in Metals," *Proc. R. Soc. London Ser. A* 275: 47-57 (1963).
15. D. E. Rimmer and A. H. Cottrell, "The Solution of Inert Gases in Metals," *Philos. Mag.* 2: 1345-53 (1957).

16. D. J. Reed, "A Review of Recent Theoretical Developments in the Understanding of the Migration of Helium in Metals and its Interaction With Lattice Defects," *Rad. Effects* 31: 129-47 (1977).
17. A. F. Rowcliffe, G.J.C. Carpenter, H. F. Merrick, and R. B. Nicholson, "An Electron Microscope Investigation of High Temperature Embrittlement of Irradiated Stainless Steel," pp. 161-99 in *Effect of Radiation on Structural Materials*, Am. Soc. Test. Mater. Spec. Tech. Publ. 426, American Society of Testing and Materials, Philadelphia, Pa., 1967.
18. W. R. Martin and J. R. Weir, "Solutions to the Problems of High Temperature Irradiation Embrittlement," pp. 440-57 in *Effect of Radiation on Structural Materials*, Am. Soc. Test. Mater. Spec. Tech. Publ. 426, American Society of Testing and Materials, Philadelphia, Pa., 1967.
19. P. J. Maziasz and T. K. Roche, "Microstructural Characterization of As-Received Prime Candidate Alloy and Examination of Microstructural Sensitivity to Fabrication and Processing Variables," *ADIP Quart. Prog. Rep. January-March* 1979, DOE/ET-0058/5, pp. 36-62.
20. P. J. Maziasz, Oak Ridge National Laboratory, unpublished data.
21. R. S. Nelson, J. A. Hudson, and D. J. Mazey, "The Stability of Precipitates in an Irradiation Environment," *J. Nucl. Mater.* 44: 318-30 (1972).
22. Personal communication, A. F. Rowcliffe, Oak Ridge National Laboratory, July 1976.

4. PATH B ALLOY DEVELOPMENT — HIGHER STRENGTH Fe–Ni–Cr ALLOYS

Path B alloys are the Fe–Ni–Cr "superalloys" in which tensile, creep–rupture, and fatigue strength levels higher than attainable in the austenitic stainless steels are achieved by precipitation of one or more phases. Many alloys in this class exhibit low swelling in fast–reactor irradiations. The technology for use of path B alloys in neutron radiation environments is not as advanced as for path A alloys. A basis to select a specific alloy type for further development is lacking. Accordingly, the ADIP task group has selected five base research alloys that are representative of the basic systems of path B alloys and deserve consideration for fusion reactor applications. The systems under investigation include γ' strengthened–molybdenum modified, γ' strengthened–niobium–modified, $\gamma'\gamma''$ strengthened, and a highnickel precipitation–strengthened alloy (–75% Ni).

Near–term activities are focused on evaluating the effects of a fusion reactor neutron spectrum on key mechanical and physical properties. Damage created by the fusion reactor neutron spectrum is approximated by fission reactor irradiation. Data are presently being obtained on a limited number of commercial alloys on which scoping studies were initiated two to three years ago. The emphasis will shift to base research alloys as they become available. For those properties that are either inadequate or degraded to an unacceptable level, the influence of composition and microstructure on the response will be examined. The research program will be oriented toward determination of mechanisms responsible for the observed property changes and the effects of metallurgical variables on the response. The objective is to develop a basis for selection of the path B prime candidate alloy(s).

5. PATH C ALLOY DEVELOPMENT — REACTIVE AND REFRACTORY ALLOYS

Two distinct and separate subgroups fall under the broad classification of path C alloys. These subgroups are conveniently classified as "reactive metal alloys" and "refractory metal alloys." Analyses of the properties required for performance of materials in high-flux regions of fusion reactors and assessments of the known and extrapolated properties have identified titanium alloys of the reactive metal alloys and vanadium and niobium alloys of the refractory metal alloys as having the most promise for fusion reactor applications. For both the reactive and refractory alloys, there is an extreme lack of data that are relevant and necessary for selection of specific alloy types for development (i.e., solid solution, precipitation strengthened, single or multiphase). In the case of titanium alloys, the most critical deficiency is the lack of data on the response of these alloys to high-fluence neutron radiation. For vanadium and niobium alloys, while the effects of radiation on mechanical behavior are not adequately known, perhaps the most alarming deficiency is the near total lack of base-line information on the effects of cyclic (fatigue) loading on mechanical performance. Precisely because of these deficiencies in the data base and overall metallurgical experience, these alloys are still in a "scoping study" phase of their evaluation as candidates for fusion reactor first-wall materials.

The ADIP task group has selected four titanium alloys, three vanadium alloys, and two niobium alloys for the scoping phase of the development program. Titanium alloys are generally classified according to the relative amounts of α (hcp) and β (bcc) phases that they contain. The titanium alloys selected represent the three alloys (types α plus β , α rich, and β rich). Vanadium and niobium alloys are not in commercial use as are the other alloy systems in the program. Selection of the scoping alloys was based primarily on results of previous programs on vanadium cladding development for LMFBRs and high-temperature alloys for space power systems. The three vanadium alloys are V-20% Ti, V-45% Cr-5%Ti, and Vanstar 7. The binary has relatively good fabricability, and appears to be swelling resistant in fast-reactor irradiations but

is rather weak. The ternary V-15% Cr-5% Ti and precipitation-strengthened Vanstar 7 alloys are significantly stronger. The Nb-1% Zr binary alloy is included as a reference material, since a significant amount of data exists for this alloy irradiated in fast reactors. The alloy Nb-5% Mo-1% Zr is much stronger than the binary and can be developed for applications near 800°C.

Near-term activities on path C alloys will focus on obtaining data on the unirradiated mechanical properties, corrosion, and compatibility, and the effects of irradiation on physical and mechanical properties. Fission reactor irradiation with and without helium preinjection, high-energy neutron sources, and charged-particle irradiations will be used in the development of techniques to approximate the effects of the fusion reactor neutron spectrum (He/dpa production). The objective is to develop sufficient understanding of the behavior of path C alloy systems (Ti, V, and Nb alloys) to allow selection of path C base research alloys. The effects of composition and microstructure on alloy performance will then be investigated in the base research alloys.

5.1 PREPARATION OF VANADIUM AND NIOBIUM PATH C SCOPING ALLOYS

R. E. Gold, R. L. Ammon, and R. W. Buckman, Jr. (Westinghouse Electric Corporation) and T. K. Roche (Oak Ridge National Laboratory).

5.1.1 ADIP Task

I.D.1 Materials Stockpile for MFE Programs (Path C)

5.1.2 Objective

The purpose of this effort is to provide sufficient quantities of the vanadium and niobium Path C Scoping Alloys to permit initial evaluation of the potential these types of alloys might offer for fusion reactor applications. Final product forms, which are to be delivered to the Oak Ridge National Laboratory Fusion Materials Stockpile, include 2.5 mm (0.10 in.) plate, 1.5 mm (0.06 in.) and 0.76 mm (0.03 in.) sheet, and 6.4 mm (0.25 in.) diameter rod.

5.1.3 Summary

Three vanadium alloy and two niobium alloy compositions are being prepared for consumable arc melting and processing to plate, sheet, and rod for the Fusion Materials Stockpile. These are the Path C (V, Nb) Scoping Alloys selected for initial evaluations as candidate fusion reactor structural materials. All melting and primary metal working operations have been completed. Extrusions to sheet bar and round bar were accomplished without difficulty; final rolling and swaging are underway. Delivery of various product forms will begin by approximately mid-August with final delivery of all materials to the Fusion Materials Stockpile at Oak Ridge expected to be complete by mid-October.

5.1.4 Progress and Status

During the current reporting period all necessary round bar and sheet bar extrusions were carried *out* for the three (3) vanadium-base and two (2) niobium-base alloys utilizing the facilities of the

Metals and Ceramics Division of the Oak Ridge National Laboratory. The alloy ingots were canned for extrusion in stainless steel; the extrusion cans were then evacuated and sealed by electron beam welding. The resulting billets, each approximately 8.0 cm (3.5 in.) in diameter, were extruded to 2.54 cm (1 in.) diameter round bar or 5.1 cm (2 in.) wide x 1.9 cm (0.75 in.) thick sheet bar at extrusion ratios of 12.2:1 and 6.4:1, respectively. All extrusions were carried out at 1200°C with no difficulty. Details of the extrusion products are summarized in Table 5.1.1. Following extrusion all materials were returned to Westinghouse for final fabrication of the sheet and rod products.

6. PATH D ALLOY DEVELOPMENT – INNOVATIVE MATERIAL CONCEPTS

Innovative material concepts are included as a path in the alloy development program because the fusion reactor environment is extremely demanding on materials in the high-flux region and the more conventional materials and metallurgical concepts may not be adequate. Novel approaches to alloy design, nonconventional material processing to tailor properties, or alternate materials such as structural ceramics and fiber composites will be considered.

7. STATUS OF IRRADIATION EXPERIMENTS AND MATERIALS INVENTORY

Irradiation experiments are presently being conducted in the ORR and HFIR, which are mixed-spectrum fission reactors, and in the EBR-II, which is a fast-spectrum reactor. Experiments are generally cooperative between several program participants. Experiment plans, test matrices, etc., are reviewed by the Alloy Development for Irradiation Performance Task Group.

The Office of Fusion Energy (ETM) of the Department of Energy has assigned program responsibility to ORNL for the establishment and operation of a central inventory of research materials to be used in the Fusion Reactor Materials research and development programs of the DOE. The primary objective is to provide a common supply of materials for use in the nationally coordinated Fusion Reactor Materials Program.

7.1 IRRADIATION EXPERIMENT STATUS AND SCHEDULE (ORNL)

The following charts show the irradiation experiment schedule, including experiments completed, in progress, and planned. Experiments are presently under way in the ORR and the HFIR, which are mixed-spectrum reactors, and the EBR-II, a fast reactor.

EBR-II subassembly X 287 has been disassembled, and the 2300 specimens are now being sorted.

ORR-MFE-II has now been repaired and has been operating satisfactorily in the ORR since May 3, 1979. A dosimetry experiment was performed during the repair and is now complete.

HFIR-CTR-23 containing fatigue specimens of Nimonic PE-16 has been disassembled. Specimens are awaiting completion of high-cycle tests on type 316 stainless steel.

The capsule design of ORR-MFE-4 has been completed. A prototype will be constructed to test the temperature control system out of reactor. The specimen racks are now being designed.

Experiment Designation	Major Objective	1977			1978			1979			1980		
		J	F	M	J	F	M	J	F	M	J	F	M
ORR-MFE-5	In-reactor fatigue crack growth experiment												
B. Experimental Breeder Reactor II													
Subassembly X 264	Effect of preinjected helium (2-200 at. ppm) on microstructure and tensile properties of 316 SS, PE-16, V and Nb alloys. Fluence $\leq 2.3 \times 10^{26}$ n/m ² , 500-825°C.												
Subassembly X 287	Effect of preinjected helium (2-200 at. ppm He) on microstructure and tensile properties of 316 SS, PE-16, V and Nb alloys. Fluence $\leq 4 \times 10^{26}$ n/m ² , 400-700°C.												
Subassembly X 217D	Stress relaxation Ti Alloys												
See footnotes [1] [2] and [3]	Effect of irradiation on swelling, tensile, fatigue, and crack growth properties of Ti scoping alloys. 370, 450, and 550°C, fluence 4.5-5.5 x 10 ²⁶ n/m ² .												

[1] EBR-II, row 2, pins B285 and B286.
 [2] Subassembly removed for EBR-II run 99.
 [3] Pin B284, row 2 for runs 96-98; row 4 for runs 100-102.

Experiment Designation	Major Objective	1977			1978			1979			1980		
		J	F	M	J	F	M	J	F	M	J	F	M
Effect of Irradiation on swelling, tensile, fatigue, and crack growth properties of V and Nb scoping alloys. EBR-II space position in reactor not yet finalized, therefore no fluence estimate.													
C. High Flux Isotope Reactor (HFIR)													
HFIR-CTR-4	PE-16 for swelling and tensile properties, 300-700°C, 2.2-4.5 dpa, 100-350 at. ppm He												
HFIR-CTR-7	PE-16 for swelling and tensile properties, 300-700°C, 9-18 dpa, 1250-3000 at. ppm He												
HFIR-CTR-8	duplicate of -7												
HFIR-CTR-9	316 and 316 + Ti for swelling and tensile properties, 280-680°C, 9-18 dpa, 400-1000 at. ppm He												

1] Earliest date irradiations can begin on present alloy development schedule.

7.2 ETM RESEARCH MATERIALS INVENTORY — F. W. Wiffen, T. K. Roche (ORNL) and J. W. Davis (McDonnell Douglas)

7.2.1 ADIP Task

ADIP Task I.D.1, Materials Stockpile for MFE Programs.

7.2.2 Purpose and Scope

The Office of Fusion Energy (ETM) of the Department of Energy has assigned program responsibility to ORNL for the establishment and operation of a central inventory of research materials to be used in the Fusion Reactor Materials research and development programs of the DOE. The primary objective is to provide a common supply of materials for use in the nationally coordinated Fusion Reactor Materials Program. This will minimize unintended materials variables and provide for economy in procurement and for centralized recordkeeping. Initially this inventory is to focus on materials related to first-wall and structural applications and related research, but various special-purpose materials may be added in the future. It is recognized that materials supplementary to this inventory will be introduced to the ETM programs from time to time, and records of those materials shall be made available to ORNL and incorporated in the records of the ETM Research Materials Inventory.

The use of materials from this inventory for research that is coordinated with or otherwise related technically to the Fusion Reactor Materials Program of DOE but which is not an integral or directly funded part of it is encouraged, with the understanding that the results of such research be made available to the Fusion Reactor Materials Program.

7.2.3 Materials Requests and Release

Materials requests must provide a statement of the programmatic end use and agreement that characterization information developed by the user shall be supplied to the inventory records. Request for materials shall be directed to ETM Research Materials Inventory at ORNL (Attention: F. W. Wiffen). Materials will be released directly if:

(a) The material is to be used for programs funded by ETM, with goals consistent with the approved Materials Program Plans of the Materials and Radiation Effects Branch.

(b) The requested amount of material is available, without compromising other intended uses.

Materials requests that do not satisfy both (a) and (b) will be discussed with the staff of the Materials and Radiation Effects Branch, Office of Fusion Energy, for agreement on action.

7.2.4 Records

Chemistry and materials preparation records are maintained for all inventory material. All materials supplied to program users will be accompanied by summary characterization information.

1.2.5 Summary of Current Inventory (June 1979)

7.2.5.1 Path A Alloys

1. Reference alloy — type 316 stainless steel. Bar, plate, rod, and 0.180-in.-diam tubing are in stock. Kework will be scheduled as required.
2. Prime Candidate Alloy (PCA) (Fe-16 Ni-14 Cr-2 Mo-Mn, Ti, Si, C). All the PCA has been delivered to OKNL by the vendor, Teledyne Allvac. Table 7.2.1 lists the product forms in stock.
3. PCA Tube production and remelt for composition variation is planned for late FY 1979.

7.2.5.2 Path B Alloys

4. A reference heat of PE-16 is in stock at ORNL. Plate, rod, and 0.180-in.-diam tubing are available.
5. Base Research Alloys

<u>Alloy</u>	<u>Ni</u>	<u>Cr</u>	<u>Mo</u>	<u>Nb</u>	<u>Ti</u>	<u>Al</u>	<u>Si</u>
B-1	25	10	1		3	1.5	0.3
B-2	40	12	3		1.5	1.5	0.3
B-3	30	12		2	2	0.5	0.3
B-4	40	12		3	1.8	0.3	0.3
B-6	75	15		1	2.5	1.5	0.3

Table 7 2 1 Material Receipts into the ERM Research Materials Inventory^a

Alloy	Heat	Product Form ^b	Dimensions			Quantity			
			(mm)	(in.)	(kg)	(lb)	(m)	(ft)	(pieces)
Path A PCA									
	K-2E0	RCS bar	130	5					1 ^c
		Round bar	100	4	417	920			
		Round bar	33	1 5/16	74	164	11	35	
		Round bar	12 06	0.475	63	138	69	227	
		Plate	13 x 130	1/2 x 5	70	154	4 6	15	
Path B BRA									
B-1	J-270	RCS bar	100	4	93	204			2
	J-271	RCS bar	100	4	91	200			2
B-2	J-268	RCS bar	100	4	98	217			2
	J-269	RCS bar	100	4	99	219			2
B-3	J-266	RCS bar	100	4	92	202			2
	J-267	RCS bar	100	4	93	204			2
B-4	J-264	RCS bar	100	4	92	202			2
	J-265	RCS bar	100	4	93	204			2
B-6	J-262	RCS bar	100	4	89	197			2
	J-263	RCS bar	100	4	83	184			2

^aAll from Venpos Telephone Allnac

^bRCS = round-corner square.

^cOne 13-mm (1/2-in.) slice from bar.

Two 140-kg (300-lb) heats of each alloy were purchased from Teledyne Allvac. This material was delivered to ORNL in September 1978, and the yield was approximately 180 kg (400 lb) per alloy.

Secondary breakdown has begun. A single sheet bar and a rod have been extruded from each of the five alloys, and the material is being used to determine thermomechanical treatment to produce final product form.

Table 7.2.1 lists the available primary product forms of the five alloys. Chemical analysis and metallography of each alloy are given in Sect. 4.2 of this report.

7.2.5.3 Path C Alloys (Refractory Alloys)

6. Small amounts of several niobium- and vanadium-base alloys are currently available at ORNL. Quantity and product forms are limited.
7. An order has been placed for the purchase of approximately 6 kg each of five alloys. Only sheet and rod will be produced.

Alloys: Nb-1% Zr

Nb-5% Mo-1% Zr

V-20% Ti

V-15% Cr-5% Ti

V-9% Cr-3.3% Fe-1.3% Zr-0.05% C (Vanstar 7)

Delivery of material is expected in the late summer of 1979.

7.2.5.4 Path C Alloys (Reactive Alloys)

8. The titanium-base scoping alloys have the following compositions, wt %:

<u>Alloy</u>	<u>Al</u>	<u>V</u>	<u>Nb</u>	<u>Zr</u>	<u>Sn</u>	<u>Cr</u>	<u>Si</u>
Ti-64	6	4					
Ti-6242s	6		2	4	2		0.09
Ti-5621s	5		1	2	6		0.25
Ti-38644	3	a	4	4		6	

At least 0.75 m² (1200 in.²) of each of these alloys is currently available in 0.76-mm (0.030-in.) thickness. This sheet is from the same heat as material currently in reactor experiments. Larger section sheet of alloy Ti-5621s is also available.

Orders are now being developed to purchase new stocks of these alloys in several product forms. Delivery dates have not yet been determined.

The titanium-base alloys are stored at McDonnell Douglas. However, inventory control and materials release are handled by ORNL, and requests should be addressed to ORNL.

8. CORROSION TESTING AND HYDROGEN PERMEATION STUDIES

Corrosion, erosion, and mass transfer are processes that may degrade mechanical properties, alter heat transfer characteristics of heat transport systems, and present maintenance problems when radioactive nuclides are involved. The importance of hydrogen permeation and the behavior of hydrogen in the alloy systems under development is clear from consideration of tritium inventory, containment, etc. In the early stages of the development program, base-line information is required to define compatible or noncompatible alloy systems and coolants. As optimized alloys are developed, more detailed data on effects of adjustments in alloy composition or structure may be required. Extensive engineering compatibility data will be required on the final optimized alloys.

- 8.1 CORROSION IN STATIC LITHIUM: FURTHER TESTS ON CORROSION INHIBITION OF TYPE 316 STAINLESS STEEL AND THE CORROSION OF WELD SPECIMENS OF TYPE 316 STAINLESS STEEL AND PATH B-LIKE MATERIALS —
P. F. Tortorelli and J. H. DeVan (ORNL)

8.1.1 ADIP Task

ADIP Task I.A.3, Perform Chemical and Metallurgical Compatibility Analyses.

8.1.2 Objective

The purpose of this program is to determine the chemical compatibility of fusion reactor candidate materials with metallic lithium. Specimens are exposed to static lithium-containing selected solute additions to identify the kinetics and mechanisms that govern corrosion by lithium. Specific program objectives are: (1) to determine the effects of N, C, H, and O on apparent solubilities in lithium, (2) to determine the C and N partitioning coefficients between alloys and lithium, (3) to determine the effects of soluble (Ca, Al) and solid (Y, Zr, Ti) active metal additions on corrosion by lithium, and (4) to determine the tendencies for dissimilar-metal mass transfer.

8.1.3 Summary

Type 316 stainless steel was exposed to Li-2 wt % N-5 wt % Al between 500 and 700°C for 1000 h. While this amount of nitrogen normally enhances attack of type **316** stainless steel, the addition of aluminum prevented significant corrosion. We studied the corrosion resistance of unstressed welds of type 316 stainless steel and two Path B-like alloys (alloys 800 and 600) in lithium. In general, after 1000 h at 500 and 600°C the welds of the three were as compatible with static as-purified lithium as their respective base alloys.

8.1.4 Progress and Status

Previous work¹ has shown that the presence of a significant amount of nitrogen in static lithium at 500 to 700°C resulted in severe corrosion

of type 316 stainless steel relative to tests in as-purified lithium. We also have found^{2,3} that additions of aluminum to static and flowing lithium effectively inhibited corrosion of type 316 stainless steel. Accordingly, we conducted experiments to determine if aluminum additions would reduce the corrosion of this steel by Li-2 wt % N. Type 316 stainless steel coupons were exposed to static Li-2 wt % N-5 wt % Al at 500, 600, and 700°C for 1000 h. The resulting weight changes are given in Table 8.1.1, which also contains data from earlier tests with Li-2 wt % N for comparison. The presence of aluminum with nitrogen in the lithium completely eliminated the large weight losses suffered by type 316 stainless steel when exposed to nitrogen alone in lithium. Specimens are now being examined metallographically to determine if the aluminum produced the same intermetallic layer on the stainless steel as observed in the absence of nitrogen.³ We are **also** checking the possibility that the beneficial effect of aluminum could have occurred by direct reaction with the nitrogen rather than by formation of a protective intermetallic layer. However, chemical analysis of the post-test lithium, which showed both a decrease in the aluminum concentration of the lithium during test from 5.0 to about 3.5 wt % and higher nitrogen concentrations relative to tests in Li-2 wt % N, indicated that the surface layer reaction was dominant.

Table 8.1.1. Weight Changes of Type 316 Stainless Steel Exposed to Static Li-2 wt % N and Li-2 wt % N-5 wt % Al for 1000 h

Temperature (°C)	Weight Change, g/m ²	
	Li-2 wt % N	Li-2 wt % N-5 wt % Al ^a
500	-51.5	+1.5, +1.5
600	-39.0	+3.4, +3.4
700	-51.0	+16.2, +9.5

^aTwo tests were run at each temperature.

We have also begun an investigation of the susceptibility of welds and weld-heat-affected zones of Fe-Cr-Ni alloys to attack by static lithium. In the preceding quarterly progress report,⁴ we reported that alloy 600 welds (with 82T filler wire) were not selectively attacked by lithium between 500 and 700°C. Subsequently, tests were performed to qualitatively study the inherent corrosion resistance of unstressed welds of type 316 stainless steel and alloys 800 and 600. These last two alloys were tested since they were readily available and had compositions that, for our purposes, were reasonably close to those of ADIP alloys B2 and B6. The weld corrosion coupons were made by taking 25- by 19- by 1.2-mm samples, cutting them in half lengthwise, setting the halves at 90° to one another, and then welding each set of halves together along their lengths. These coupons were then sealed in type 316 stainless steel capsules with as-purified lithium and exposed for 1000 h at 500, 600, and 700°C. The resulting weight changes are listed in Table 8.1.2. It is interesting to note that the alloy 800 specimens suffered the greatest weight losses. This is consistent with the metallographic examinations that showed that this alloy was attacked to a greater degree than alloy 600 and type 316 stainless steel (see Fig. 8.1.1-3). This result is somewhat surprising since the alloy with

Table 8.1.2. Weight Changes of Weld Coupons Exposed' to Static Lithium for 1000 h

Temperature (°C)	Weight Change, g/m ²		
	316 SS ^b	Alloy 800 ^c	Alloy 600 ^c
500	-3.3, -3.0	-13.9, -12.7	-3.5, -1.8
600	-3.0, -2.3	-49.5, -47.8	-3.2, -3.1
700	-2.5, -1.7	-418.1, -420.5	-19.3, -1.9

^aTwo tests were run for type of material at each temperature.

^bType 316 stainless steel weld wire was used.

^c82T weld wire (72% Ni-20% Cr-3% Mn-1% Fe) was used.

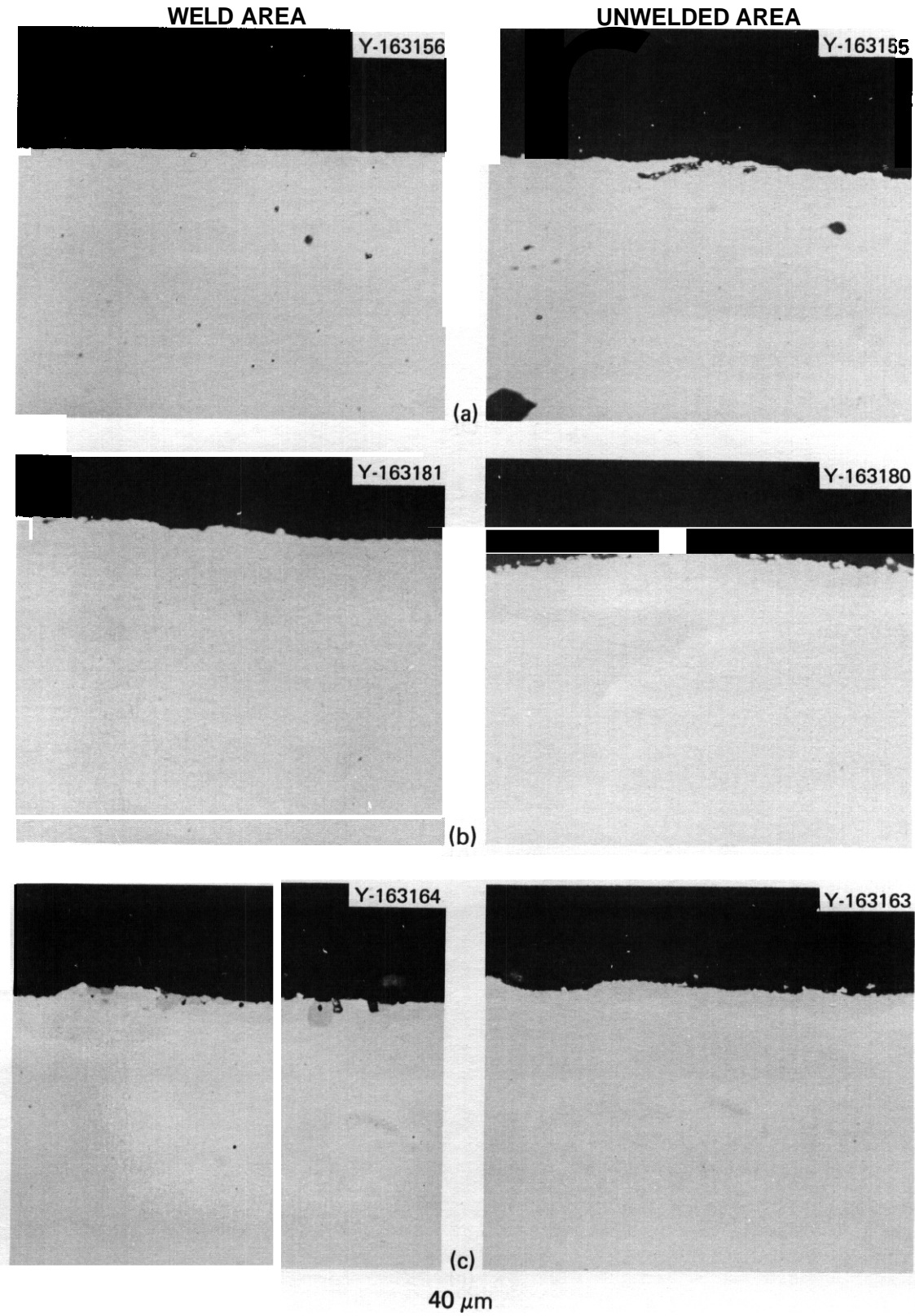


Fig. 8.1.1. Exposure for 1000 h to Static Lithium at 500°C.
(a) Type 316 stainless steel. (b) Alloy 800. (c) Alloy 600.

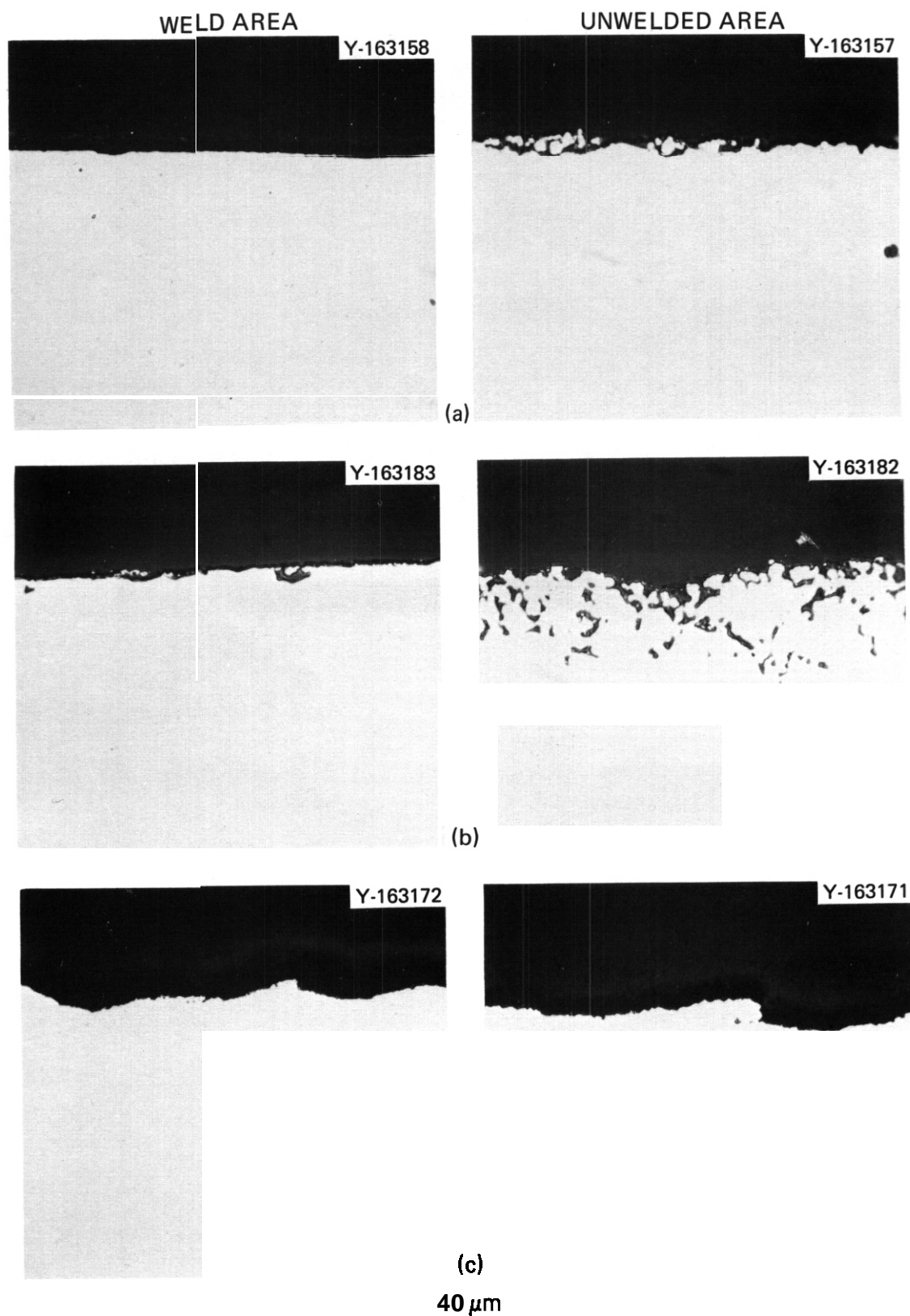


Fig. 8.1.2. Exposure for 1000 h to Static Lithium at 600°C.
 (a) Type 316 stainless steel. (b) Alloy 800. (c) Alloy 600.

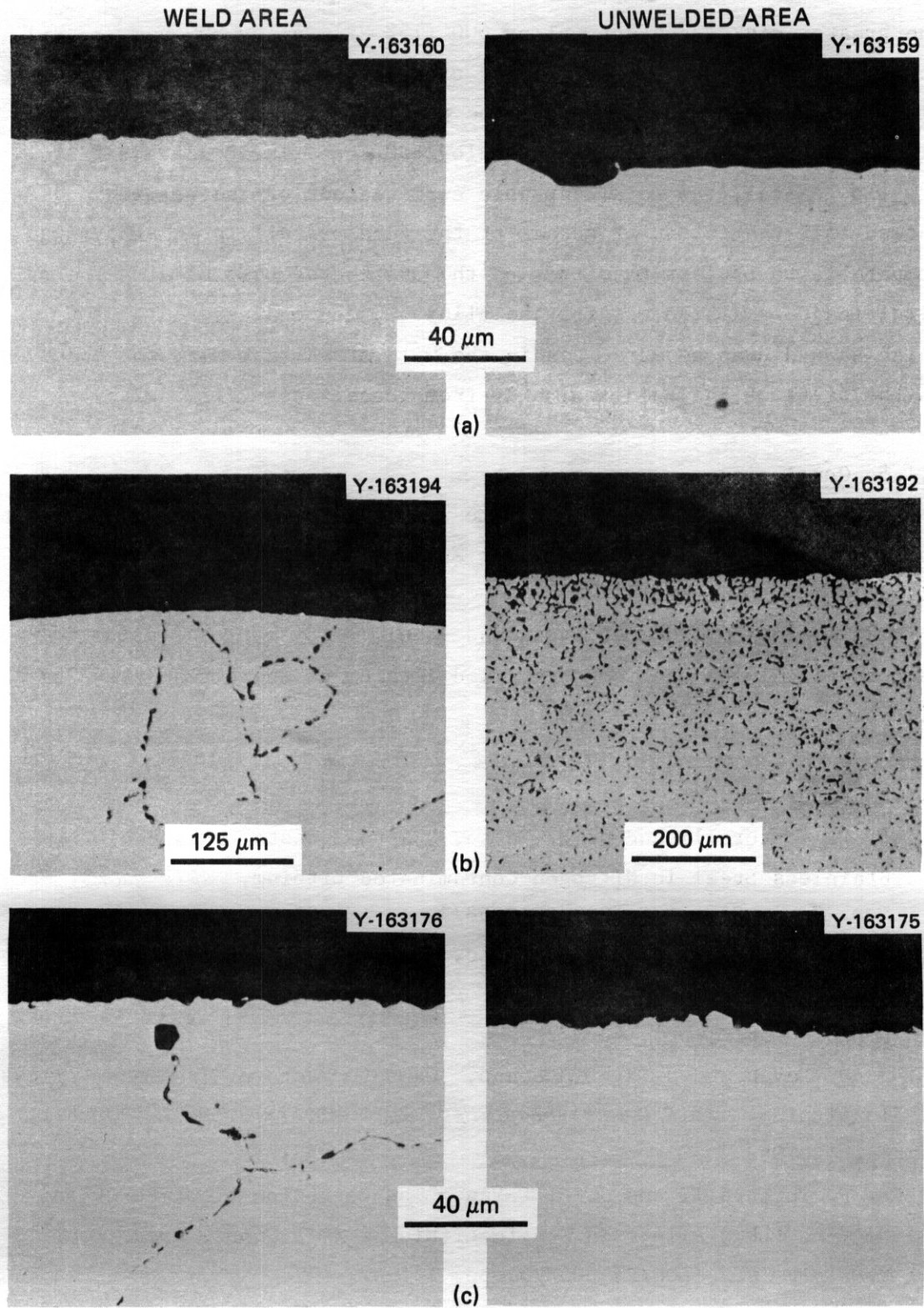


Fig. 8.1.3. Exposure for 1000 h to Static Lithium at 700°C.
(a) Type 316 stainless steel. (b) Alloy 800. (c) Alloy 600.

the greater nickel content, alloy 600 (75% Ni) (alloy 800 has 32% Ni), would be expected to have a greater dissolution rate. In previous tests with unwelded corrosion coupons, the corrosion of alloy 600 in static lithium was greater than that of alloy 800.

In general, the metallographic examinations of the weld coupons showed that the extent of attack of the welds of all three alloys was comparable to or less than that of the unaffected base metal. The only significant exception was for the alloy 600 coupons exposed at 700°C, which showed deep penetrations in the weld areas that were not observed on the parts of the specimens away from these zones (Fig. 8.13).

8.1.5 Conclusions

1. The addition of aluminum to static lithium effectively inhibits the corrosion of type 316 stainless steel, regardless of the amount of nitrogen in the lithium.

2. Welds of type 316 stainless steel, alloy 800, and alloy 600 are as compatible with static as-purified lithium as their respective base alloys.

8.1.6 References

1. P. F. Tortorelli and J. H. DeVan, "Capsule Tests of Type 316 Stainless Steel in Nitrogen-Contaminated Lithium," *ADIP Quart. Prog. Rep. Sept. 30, 1978*, DOE/ET-0058/3, pp. 84-91.
2. P. F. Tortorelli and J. H. DeVan, "Capsule Tests of Iron-Base Alloys in Lithium," *ADIP Quart. Prog. Rep. June 30, 1978*, DOE/ET-0058/2, pp. 148-57.
3. J. H. DeVan and J. R. DiStefano, "Capsule Tests of Iron-Base Alloys in Lithium," *ADIP Quart. Prog. Rep. Mar. 31, 1978*, DOE/ET-0058/1, pp. 190-99.
4. P. F. Tortorelli and J. H. DeVan, "The Corrosion of Ni-Fe-Cr and Co-V-Fe (LR0) Alloys in Static Lithium," *ADIP Quart. Prog. Rep. Mar. 31, 1979*, DOE/ET-0058/5, pp. 141-47.

8.2 MASS TRANSFER DEPOSITS IN LITHIUM-TYPE 316 STAINLESS STEEL THERMAL-CONVECTION LOOPS — P. F. Tortorelli and J. H. DeVan (ORNL)

8.2.1 ADIP Task

ADIP Task I.A.3, Perform Chemical and Metallurgical Compatibility Analyses.

8.2.2 Objective

The purpose of this task is to evaluate the corrosion resistance of possible first-wall materials to flowing lithium in the presence of a temperature gradient. Corrosion rates (in terms of both dissolution and deposition) are measured as functions of time, temperature, additions to the lithium, and flow conditions. These measurements are combined with chemical and metallographic examinations of specimen surfaces to establish the mechanisms and rate-controlling processes for dissolution and deposition reactions.

8.2.3 Summary

We studied the morphology and composition of mass transfer deposits in lithium-type 316 stainless steel thermal-convection loops (TCLs). Initially the deposits were needle-like crystals of nearly pure chromium. After longer operating times the deposits were blocky, and their composition varied as a function of their distance above the original surface. The later-formed deposits contained iron, chromium, and nickel. However, they were enriched in chromium and nickel relative to the concentrations of these two elements in the stainless steel. A plug that formed in a TCL after 9000 h consisted of lithium and a tangle of chromium crystals.

8.2.4 Progress and Status

As described previously¹ TCLs are being used to study the compatibilities of materials with flowing lithium. Several type 316 stainless steel TCLs in the form of 0.48- by 0.76-m parallelograms have circulated lithium between 600 and 450°C for up to 10,000 h. Under such conditions

material is dissolved in the hot zone of a loop and is transferred to colder areas of the circuit. The subsequent accumulation of deposits in the colder regions tends to be more serious than the loss of structural material in higher temperature areas. An example of this is in the preceding quarterly,² which reported that two of our TCLs were plugged by mass transfer deposits. Because of their importance in liquid metal systems, we have conducted a limited study of the morphology and composition of such deposits.

We have examined deposits on coupons located in the lower temperature (450–500°C) areas of two TCLs; one operated for 1700 h and the other circulated lithium for 10,000 h. The deposits on the coupons exposed for 1700 h were needle-like crystals (see Fig. 8.2.1) that had an approximate composition of 95% Cr, 5% Ni, and less than 1% Fe. In contrast to this the deposits on coupons that had been in flowing

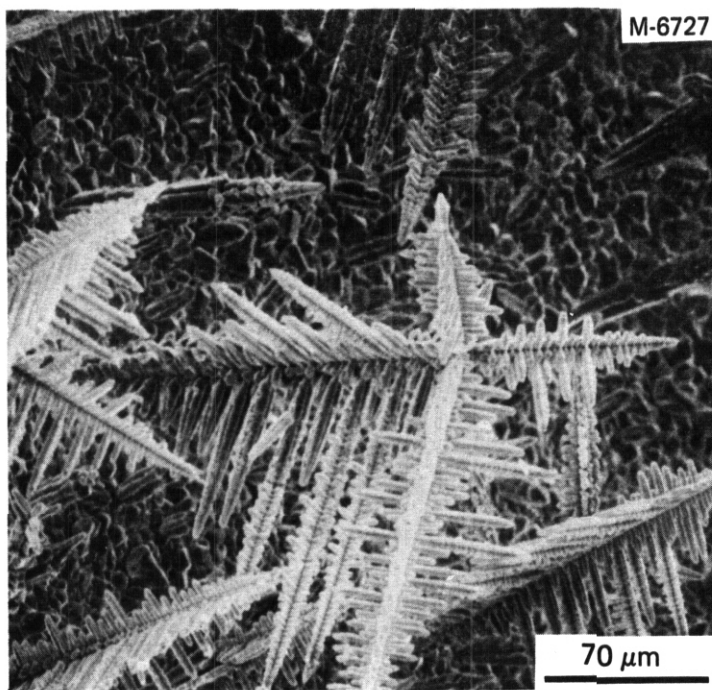


Fig. 8.2.1. Deposits that Formed on a Coupon in a Lithium-Type 316 Stainless Steel Thermal-Convection Loop at 2450°C After 1700 h.

lithium for 9000 h had a different morphology (see Fig. 8.2.2). The deposits were "blocky" and tended to pile up on one another. Energy dispersive x-ray analysis of these surfaces showed that the composition of the deposits varied: the topmost showed significant concentrations of chromium, nickel, and iron (and were enriched in chromium and nickel relative to type 316 stainless steel), while the underlying deposits tended to be similar in composition to the deposits exposed for 1700 h described above (that is, they are almost pure chromium). Electron beam microanalysis confirmed this difference in composition between layers of deposits. An example of these results is shown in Fig. 8.2.3, which shows the differences in composition between the upper and lower levels of deposits and the underlying base alloy.

In the preceding quarterly² we reported that the plug from a TCL with 10,000 h of operation appeared to be composed of lithium and small crystallites. This plug was subsequently examined in a scanning electron

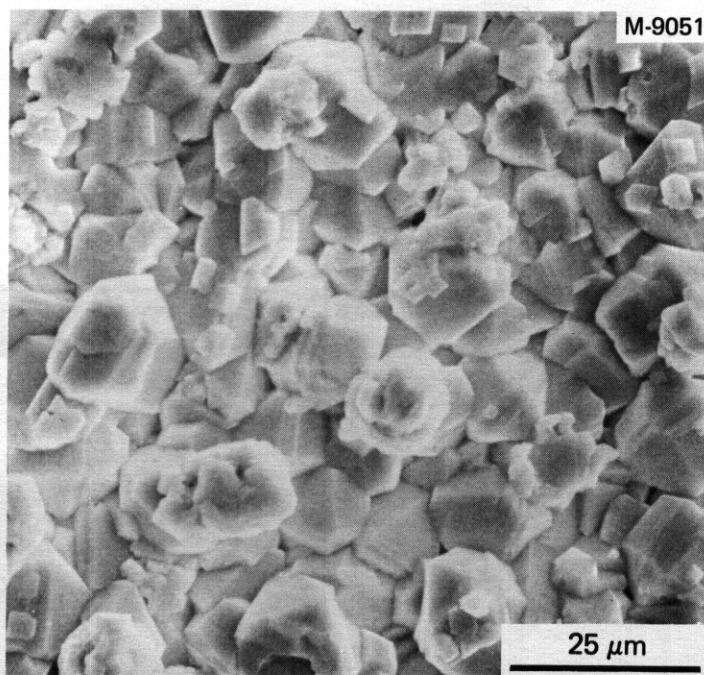
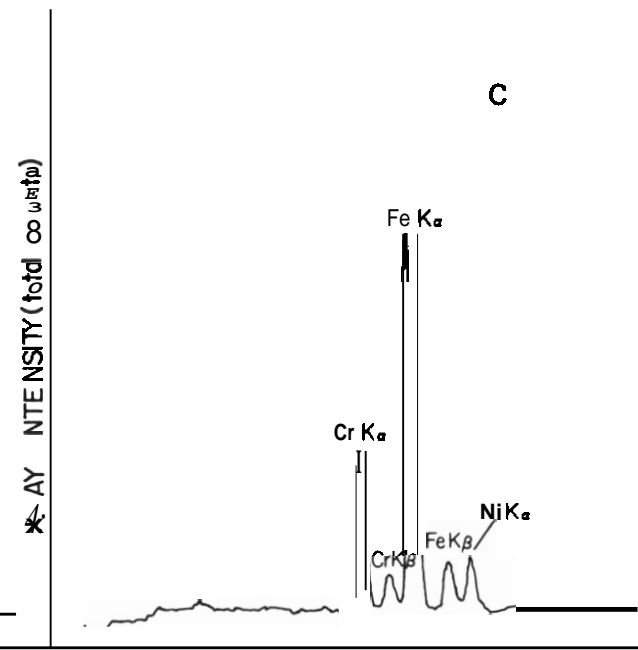
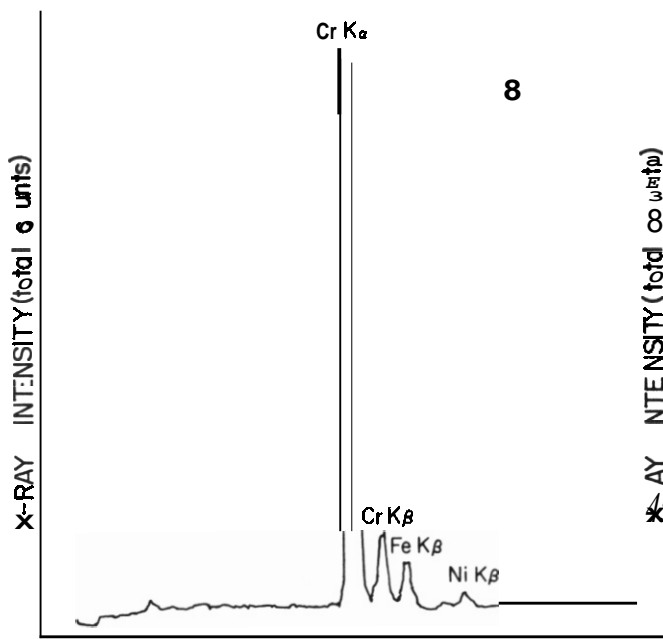
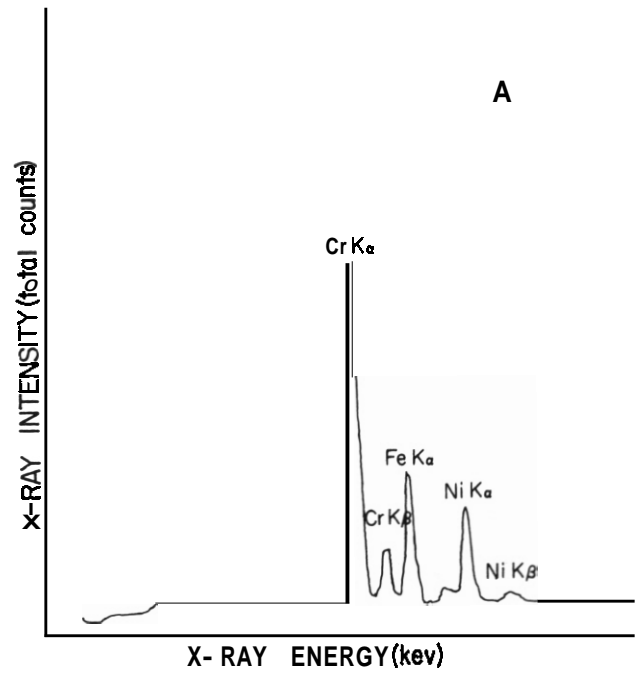
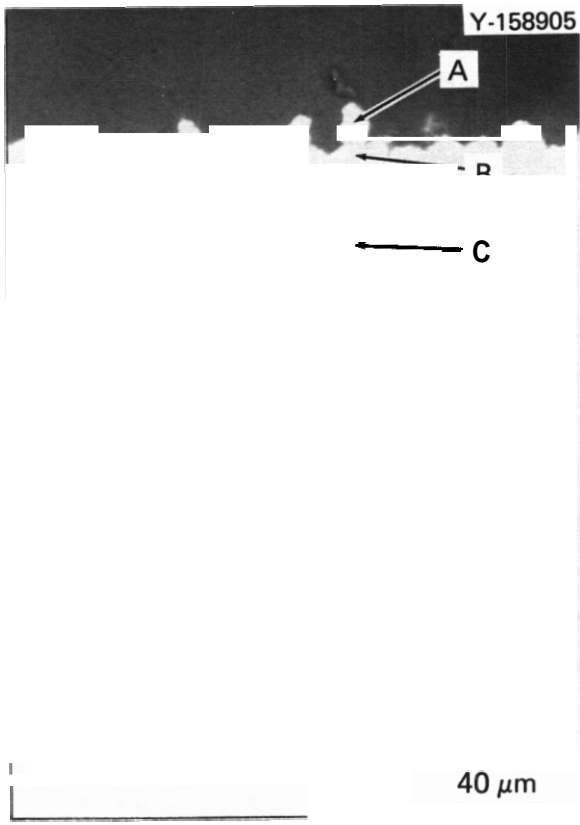


Fig. 8.2.2. Deposits that Formed on a Coupon in a Lithium-Type 316 Stainless Steel Thermal-Convection Loop at Approximately 450°C After 9000 h.



microscope, and our initial hypothesis was verified. While most of the mass was lithium, the downstream end of the plug was an aggregate of crystals (see Fig. 8.2.4) that resembled those observed on a cold leg coupon after 1700 h (see Fig. 8.2.1). Energy dispersive x-ray analysis showed that many of these crystals were principally chromium, while the rest contained chromium and nickel in large concentrations.

In view of the above observations, we can qualitatively describe the mass transfer and deposition process. Initially, solids enriched in chromium are precipitated from the lithium in the colder regions of the circuit. These are of the form shown in Fig. 8.2.1. Eventually, as the initially high dissolution rates of chromium and nickel in the hot zone decrease relative to the iron dissolution rate,³ the composition of the later-forming deposits starts to more closely approach that of stainless steel; that is, the relative amounts of iron and nickel in the deposits increase. The plug from the TCL operated for 10,000 h was chiefly caused

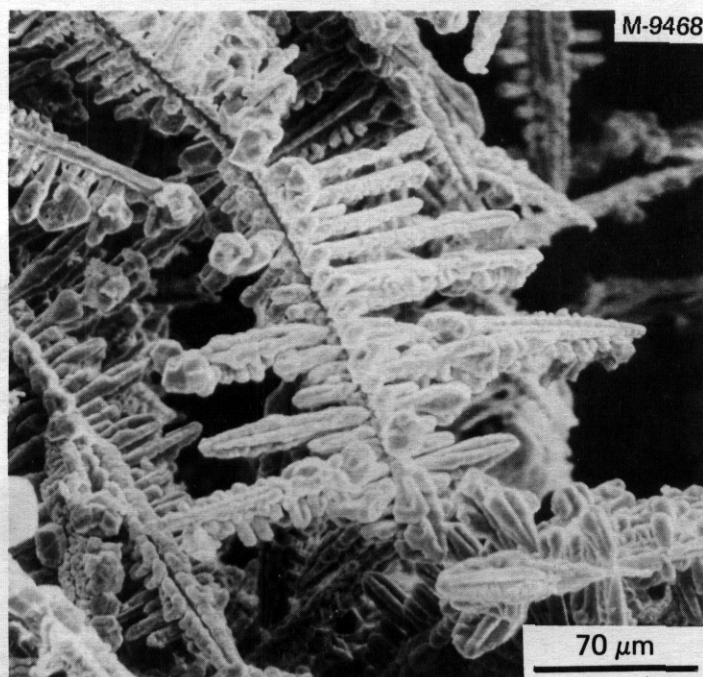


Fig. 8.2.4. Crystals Found in a Mass-Transfer Plug from a Lithium-Type 316 Stainless Steel Thermal-Convection Loop that had Operated for 10,000 h.

by a **mass** of chromium-rich crystals. Therefore, it seems that during operation of a lithium loop the initial chromium crystallites **can** be dislodged from various surfaces and can be carried to a point in the circuit where they can aggregate and severely restrict flow.

8.2.5 Conclusions

1. In lithium-type 316 stainless steel circuits, nearly pure ~~reedle-~~like chromium crystals are initially formed in the colder parts of the loops. These crystals can eventually form aggregates that can severely restrict the flow of lithium.

2. At longer operating times the morphology and composition of the mass transfer deposits change. The deposits contain significant amounts of iron, nickel, and chromium with the last two elements in greater relative concentrations than in normal type 316 stainless steel.

8.2.6 References

1. J. H. DeVan and J. R. DiStefano, "Thermal-Convection Loop Tests of Type 316 Stainless Steel in Lithium," *ADIP Quart. Prog. Rep.* Mar. 31, 1978, DOE/ET-0058/1, pp. 200-08.
2. P. F. Tortorelli and J. H. DeVan, "Corrosion in Lithium-Type 316 Stainless Steel Thermal-Convection Systems," *ADP Quart. Prog. Rep.* Mar. 31, 1979, DOE/ET-0058/5, pp. 148-55.
3. P. F. Tortorelli and J. H. DeVan, "Thermal-Gradient ~~Mass~~ Transfer in Lithium-Stainless Steel Systems," paper presented at First Topical Meeting on Fusion Reactor Materials, Miami Beach, Fla., Jan. 1979 (to be published in the *Journal of Nuclear Materials*).

8.3 HYDROGEN DISSOLUTION AND PERMEATION CHARACTERISTICS OF TITANIUM-BASE ALLOYS - E. H. Van Deventer, and V. A. Maroni (Argonne National Laboratory).

8.3.1 ADIP Task

I.A.4. Hydrogen Dissolution and Permeation Effects. The results presented in this section contribute to Subtask I.A.4., Milestones I.A.b. and I.A.c.

8.3.2 Objective

The objective of the work reported in this section is to provide base-line hydrogen dissolution and permeation data for the group of titanium-base alloys currently under examination as part of the ADIP Path C alloy development activities. The hydrogen dissolution, outgassing and permeation characteristics of this family of materials is vital to an understanding of their performance as first-wall and blanket structural materials for fusion devices. A further objective of this work is to begin examining methods for overcoming any serious hydrogen isotope uptake and migration problems associated with the rather strong hydride-forming nature of titanium and its alloys.

8.3.3 Summary

The hydrogen permeation characteristics of an anodized sample of Ti-6Al-4V were measured from 450 to 665°C for hydrogen driving pressures in the range from 0.2 to 17 Pa. The permeability of the anodized sample was found to be about the same as that of the ion-nitride coated sample of Ti-6Al-4V studied previously, and about an order of magnitude lower than that of pure Ti-6Al-4V. A least-squares analysis was conducted on data for pure Ti-6Al-4V, ion-nitride-coated Ti-6Al-4V, and anodized Ti-6Al-4V wherein the preexponential term and the activation energy were varied independently for each sample but a common refined value for the pressure exponent was sought. It is clear from the results of this analysis that the coating procedures caused a measurable but far less than desirable reduction in the permeability of Ti-6Al-4V. The optimized pressure exponent, 0.64, suggests that the normally-assumed bulk-diffusion-limited

permeation mechanism is being affected or perhaps totally superseded by another mechanism involving the surfaces of the alloy.

8.3.4 Progress and Status

The hydrogen permeation characteristics of a sample of Ti-6Al-4V that had been anodized on both surfaces (by McDonnell Douglas Astronautics Co.) were measured from 450 to 665°C for hydrogen driving pressures in the range from 0.2 to 17 Pa. The permeability of the anodized sample (based on 25 data points) was found to be about the same as that of the ion-nitride coated sample of Ti-6Al-4V studied previously', and about an order of magnitude lower than that of pure Ti-6Al-4V. The permeabilities of all of the Ti-base alloys (coated and uncoated), studied over the past year, have ranged from being several hundred to being several thousand times greater than those of 300-series stainless steels.

A detailed mathematical study of all of the data obtained for the various modifications of Ti-6Al-4V investigated to date has been initiated and is beginning to produce results. A least-squares analysis was conducted on data for pure Ti-6Al-4V, ion-nitride-coated Ti-6Al-4V (one surface), and anodized Ti-6Al-4V (both surfaces) wherein the preexponential term and the activation energy were varied independently for each sample but a common refined value for the pressure exponent was sought. The results of this analysis are presented in Fig. 8.3.1. The shaded areas represent the overall uncertainties in both the raw data and the mathematical refinement procedure. The common pressure exponent was 0.64 with an uncertainty of less than $\pm 10\%$. Accordingly, the results in Fig. 8.3.1 are plotted against a $(\text{pressure})^{0.64}$ factor which must be kept in mind when extrapolating these results to other pressures.

It is clear from the results in Fig. 8.3.1 that the coating procedures caused a measurable but far less than desirable reduction in the permeability of Ti-6Al-4V. The optimized pressure exponent, being significantly greater than 0.5, suggests that the nonually-assumed bulk-diffusion-limited permeation mechanism is being affected or perhaps totally superseded by another mechanism which undoubtedly is taking place at the surfaces of the alloy. It is a fact that the product of the hydrogen solubility parameter and the true **bulk** diffusion parameter for

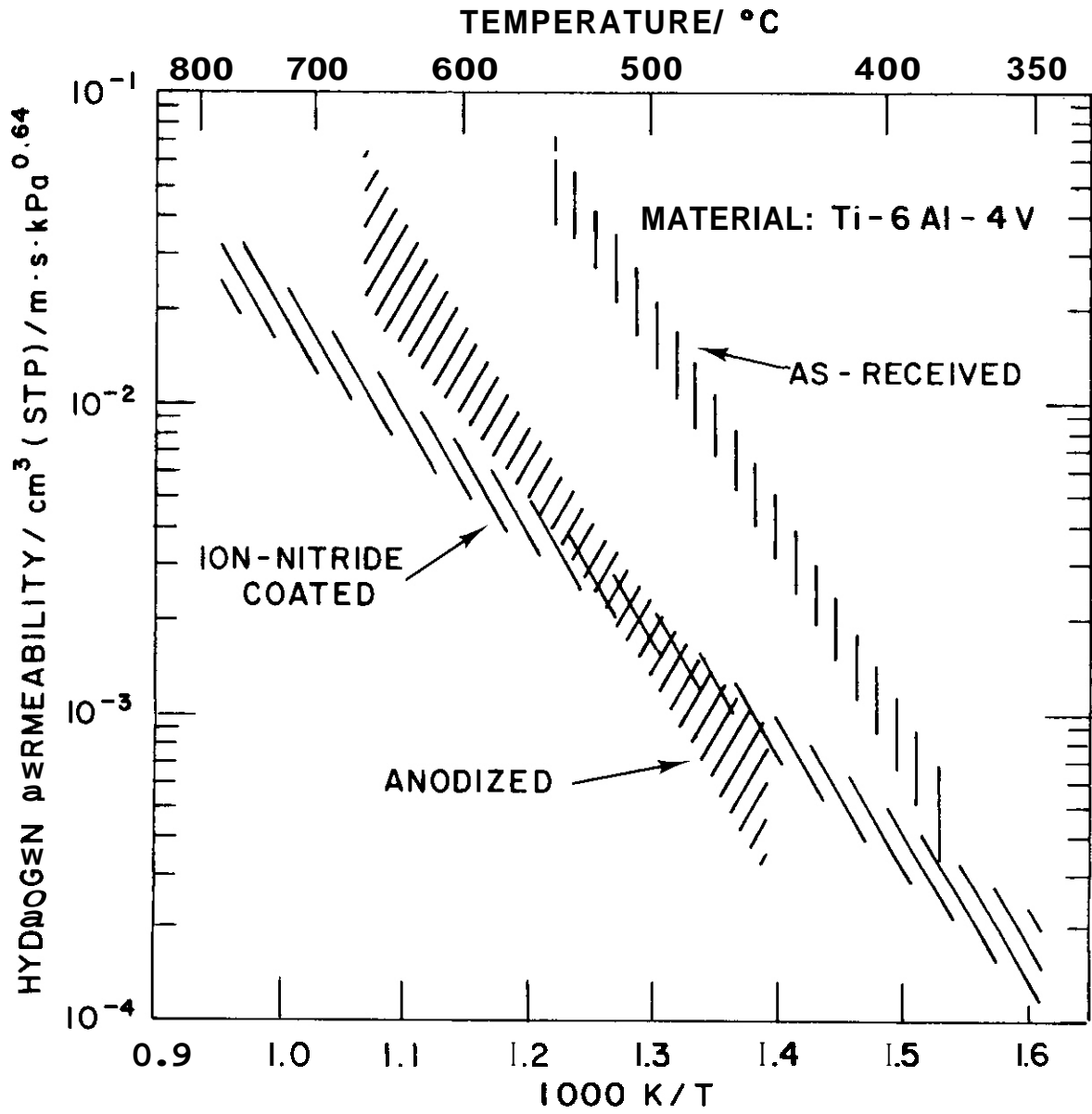


Fig. 8.3.1 Hydrogen permeation data for "as-received" and treated samples of Ti-6Al-4V.

Ti-6Al-4V at temperatures in the range shown in Fig. 8.3.1 yields a permeability significantly higher than the results shown in Fig. 8.3.1. Furthermore, the tendency of calculated permeation values based on the (solubility \times diffusion) product is to increase with decreasing temperature, primarily because the decreasing diffusion parameter is more than offset by the increasing solubility parameter at progressively lower temperatures. The permeation mechanism that has been observed for these titanium-based materials is certainly not classical and requires more study. A sample of high purity titanium metal is being readied for permeation study to determine the baseline characteristics of the unalloyed material.

8.3.5 Conclusions

See section 8.3.3.

8.3.6 References

1. E. H. Van Deventer, E. Veleckis, and V. A. Maroni, *Hydrogen Dissolution and Permeation Characteristics of Titanium-Base Alloys*, Alloy Development for Irradiation Performance Quarterly Progress Report: January-March 1979, U.S. Department of Energy Report DOE/ET-0058/5 (1979) pp. 132-140.

8.4 VANADIUM ALLOY/LITHIUM PUMPED LOOP STUDIES - D. L. Smith, R. H. Lee, and V. A. Maroni (Argonne National Laboratory).

8.4.1 ADIP Task

I.A.3. Chemical and Metallurgical Compatibility Analysis. The results presented in this section contribute to Subtask I.A.3.4, Milestones I.A.3.c, and I.A.3.d.

8.4.2 Objective

The objective of this work is to develop preliminary data on the compatibility of candidate Path C alloys exposed to a flowing lithium environment. The major effort involves investigations of nonmetallic element interactions in reactive/refractory metal-lithium systems. Information relating to atmospheric contamination of reactive/refractory metal alloys will also be generated. Specific near-term experiments include measurements on the distribution of nonmetallic elements between selected vanadium alloys and lithium, and the effects of lithium exposure on the mechanical properties of vanadium alloys. The results of this work will contribute to the data base that relates compatibility and corrosion phenomena to other alloy development activities and will provide a basis for selecting candidate alloys for further development.

8.4.3 Summary

The stainless-steel-clad vanadium-15% chromium alloy loop for studies of circulating liquid lithium has continued to operate through the third quarter of FY-1979. This 0.5-liter-capacity, forced circulation loop is being used in investigations of (1) the distribution of nonmetallic elements in lithium/refractory metal systems and (2) effects of a lithium environment on the mechanical properties of selected refractory metals. Exposure of zirconium foil to lithium at both 673 and 873 K resulted in significant pickup of nitrogen by the zirconium and a corresponding reduction of the nitrogen concentration in lithium.

8.4.4 Progress and Status

Investigations are continuing on (1) the distribution of non-metallic elements in lithium/Path C alloy systems and (2) effects of a lithium environment on the mechanical properties of selected reactive/refractory metals. Tests are being conducted in a small forced circulation stainless steel clad vanadium alloy loop. The loop has been operating without interruption for over 10 Ms (>100 days). Initial operation was at 673 K for 2 Ms. Loop temperature was then raised to 873 K where it has since been maintained. Tests to date include the taking of four filtered lithium dip samples for determinations of the nitrogen concentration in lithium, two exposures of zirconium foil and two exposures of vanadium wire. The purpose of the zirconium exposures is to reduce the nitrogen concentration in lithium by gettering and to evaluate the hydrogen concentration in the system. The latter determination will be accomplished by analyzing the hydrogen concentration in zirconium and obtaining the equivalent hydrogen pressure at equilibrium from literature data. Analysis of the nitrogen pickup in the zirconium will provide a measure of the nitrogen in the system. Table 8.4.1 summarizes results of the nitrogen analyses of the lithium. The nitrogen concentration in the lithium has been reduced from an initial value of ~1340 wppm to ~36 wppm.

Exposure of zirconium foil at 673 K for 0.43 Ms resulted in a gold tarnish indicative of ZrN on the surface. The zirconium foil exposed at 873 K for 0.60 Ms resulted in a heavier gold film on the sample. Electron microprobe analysis of this film indicated a strong nitrogen count. Quantitative analyses of the zirconium samples are in progress.

Table 8.4.1 Nitrogen Analyses of Lithium from
the Vanadium Alloy Test Loop

Sample No.	Operation Time (Ms)	Lithium Temperature (K)	Nitrogen Concentration (wppm)	Comments
VL-1	1.10	673	1342 ± 25	Represents initial concentration
VL-2	1.11	673	1325 ± 25	Duplicate sample
VL-4	5.00	871	95 ± 25	After exposure of Zr foil for 0.43 Ms at 673 K and operation at 873 K for 2.60 Ms
VL-5	6.80	873	36	After exposure of Zr foil for 0.60 Ms at 873 K

8.4.5 Conclusions

Exposure of zirconium foil to lithium contained in a vanadium alloy loop at 873 K resulted in significant transfer of nitrogen from the lithium to the zirconium. These results are in agreement with calculated trends. (1)

8.4.6 References

1. D. L. Smith and K. Natesan, "Influence of Nonmetallic Impurity Elements on the Compatibility of Liquid Lithium with Potential CTR Containment Materials," *Nucl. Technol.* **22**: 392-404 (1974).

DOE/ET-0058/6
Distribution
Category
uc-20, 20c

DISTRIBUTION

- 1-4. Argonne National Laboratory, 9700 South Cass Avenue,
Argonne, IL 60439
- L. Greenwood
V. Maroni
D. L. Smith
H. Wiedersich
- 5-6. Battelle-Pacific Northwest Laboratory, P.O. Box 999,
Richland, WA 99352
- J. L. Brimhall
D. Dingee
7. Carnegie-Mellon University, Schenley Park, Pittsburgh, PA
15213
- J. C. Williams
- 8-203. Department of Energy, Technical Information Center, Office of
Information Services, P.O. Box 62, Oak Ridge, TN 37830
- For distribution as shown in TIL)-4500 Distribution
Category, UC-20 (Magnetic Fusion Energy), and UC-20c
(Reactor Materials)
- 204-209. Department of Energy, Office of Fusion Energy, Washington, DC
20545
- M. M. Cohen
T. C. Reuther, Jr. (5 copies)
210. Department of Energy, Oak Ridge Operations Office, P.O. Box E,
Oak Ridge, TN 37830
- Office of Assistant Manager, Energy Research and Development
211. General Atomic Company, P.O. Box 81608, San Diego, CA 92138
- S. M. Rosenwasser

- 212-217. Hanford Engineering Development Laboratory, P.O. Box 1970,
Richland, WA 99352
- D. G. Doran
J. J. Holmes
R. E. Nygren
E. C. Opperman
R. W. Powell
J. L. Straalsund
- 218-219. Lawrence Livermore Laboratory, P.O. Box 808, Livermore, CA
94550
- M. Guinan
C. M. Logan
220. Massachusetts Institute of Technology, Cambridge, MA 02139
- D. J. Rose
- 221-222. McDonnell Douglas Astronautics Company, East, P.O. Box 516,
St. Louis, MO 63166
- J. W. Davis
D. L. Kummer
- 223-225. Naval Research Laboratory, Washington, DC 20375
- Superintendent, Materials Science and Technology Division
J. A. Sprague
H. Watson
- 226-253. Oak Ridge National Laboratory, P.O. Box X, Oak Ridge, TN 37830
- Central Research Library (2 copies)
Document Reference Section
Laboratory Records Department (2 copies)
Laboratory Records Department, RC
ORNL Patent Section
B. G. Ashdown
E. E. Bloom (5 copies)
D. N. Braski
J. H. DeVan
T. A. Gabriel
M. L. Grossbeck
M. R. Hill (3 copies)
K. C. Liu
P. J. Maziasz
C. J. McHargue
T. K. Roche
J. L. Scott
P. F. Tortorelli
F. W. Wiffen
J. W. Woods

254-255. Sandia Laboratories, Livermore Division 8316, Livermore, CA
94550

J. Swearengen
W. Baller

256. University of California, Department of Chemical, Nuclear, and
Thermal Engineering, Los Angeles, CA 90024

R. W. Conn

251. University of Virginia, Department of Materials Science,
Charlottesville, VA 22901

W. A. Jesser

258. University of Wisconsin, 1500 Johnson Drive, Madison, WI
53706

W. G. Wolfer

259. Westinghouse Electric Company, Fusion Power Systems Department,
P.O. Box 10864, Pittsburgh, PA 15236

R. E. Gold

